



RESEARCH ARTICLE

10.1029/2022MS003158

Key Points:

- Intermediate, eastward zonal jets are an important oxygen supply route to the oxygen minimum zones and modulate their westward extent
- Robust, intermediate zonal jets emerge in a high-resolution (3 km), basin-scale simulation with robust eddying motions at depth
- A correct representation of the zonal jets in climate models is key for reliable, long-term forecasts of ocean deoxygenation

Correspondence to:

P. H. R. Calil,
paulo.calil@hereon.de

Citation:

Calil, P. H. R. (2023). High-resolution, basin-scale simulations reveal the impact of intermediate zonal jets on the Atlantic oxygen minimum zones. *Journal of Advances in Modeling Earth Systems*, 15, e2022MS003158. <https://doi.org/10.1029/2022MS003158>

Received 22 APR 2022

Accepted 5 FEB 2023

High-Resolution, Basin-Scale Simulations Reveal the Impact of Intermediate Zonal Jets on the Atlantic Oxygen Minimum Zones

Paulo H. R. Calil¹

¹Institute of Carbon Cycles, Helmholtz-Zentrum Hereon, Geesthacht, Germany

Abstract Eastward zonal jets at intermediate depths of 300–800 m connect the oxygen-rich western boundary of the Atlantic basin with the oxygen minimum zones (OMZs) on the eastern boundary. They are not well represented in climate models because the low horizontal resolution of these models yields excessive viscosity. We use two physical-biogeochemical model configurations of the Tropical Atlantic to show that the increase in resolution results in more robust intermediate zonal jets and a better representation of the OMZs. The OMZ structure is distorted at low-resolution as surface, westward jets advect low-oxygen waters from the eastern boundary much further west than in the climatology. The emergence of robust eastward jets in the high-resolution run alleviate this problem and reproduce the Atlantic OMZs more accurately. The asymmetry between westward and eastward jets occurs because the former are associated with homogenous potential vorticity regions originating in the eastern boundary while the latter are associated with potential vorticity gradients. Intermediate, eastward jets constrain the westward expansion of the OMZs by supplying oxygen to their western edge. Within the OMZs, higher resolution allows a better representation of the boundary current system and eddying processes at depth which redistribute of low oxygen values from the productive eastern boundary. Basin-scale, high-resolution simulations reproduce more accurately the transfer of energy across scales that results in robust zonal jets as well as their impact on the ocean biogeochemistry. Accurate model predictions provide a pathway to disentangle natural and anthropogenic causes of ocean deoxygenation.

Plain Language Summary Long-term averages of ocean velocities reveal the existence of east-west, alternating currents along multiple latitudes. These currents are difficult to observe and model because of their small speeds at great depths. Despite their low intensity, in the long-term they can transport tracers across the ocean basins with oxygen being a very important one as it provides conditions for aerobic respiration in so-called oxygen minimum zones (OMZs) on the eastern side of the basin. Long-term measurements show that oxygen concentrations are decreasing in various regions of the ocean and that OMZs are expanding, which can be a problem as these regions may become inhospitable for aerobic life. That is why we need to understand the processes that supply oxygen to OMZs and are important for their evolution with time. Models can be used as tools for testing hypotheses regarding the expansion or contraction of OMZs in the future. However, models must be shown to correctly simulate the dynamics and biogeochemistry of the region as a whole. Our results show that these intermediate east-west current systems are important in structuring the OMZs and that higher-resolution, basin-scale simulations are necessary to correctly simulate their impact on oxygen concentrations in the ocean.

1. Introduction

Over the last decade, several studies have shown that regions with low oxygen concentrations are expanding over the world's oceans, a phenomenon which has been termed ocean deoxygenation (Breitburg et al., 2018; Levin, 2018; Stramma et al., 2008). These changes are driven by a combination of anthropogenic climate change and the natural variability of the ocean. As climate change warms the upper ocean it reduces oxygen solubility, increases upper ocean stratification and thus reduces oxygen mixing as well as induces changes in respiration rates (Levin, 2018). Natural ocean variability may also alter the oxygen supply as major climate fluctuations such as El Niño, the North Atlantic Oscillation and the Atlantic Meridional Mode change atmospheric and oceanic conditions over relatively long periods which makes it challenging to separate natural oscillations from long-term trends (Bryden et al., 2003). Disentangling the natural and anthropogenically-induced oxygen variability requires the use of models as prognostic or diagnostic tools, as they can be forced with different conditions which

may or may not include the effects of climate change and allow a detailed examination of specific processes. A pre-requisite for the use of models in this fashion is their ability to provide a realistic distribution of tracers and the velocity structure as compared to available observations.

The oxygen budget is a combination of physical and biological processes on coastal, shelf and open seas which vary on spatial scales of a few to thousands of kilometers and temporal scales of a few days to decades. Therefore, a thorough understanding of the system requires a multi-scale approach in which most of the important processes are adequately resolved. This is both an observational and modeling challenge. On one hand, observations are limited by repeated, relatively sparse hydrographic stations or point-wise long-term measurements. While extremely valuable in detecting and monitoring long-term changes, they do not allow a complete understanding of specific processes that modulate oxygen concentrations in oxygen minimum zones (OMZs). On the other hand, hydrodynamic models are usually limited by trade-offs between domain size, horizontal resolution and subgrid-scale parameterizations which hinder their ability to appropriately resolve all the important processes in the time-space spectrum. The coupling with biogeochemical models compounds the problem as more variables are simulated and a number of biogeochemical parameters need to be selected, adding more uncertainty to the prognostics. Long-term predictions of oxygen concentrations in the ocean are based on ensembles of climate models with sometimes divergent prognostics (Cabr e et al., 2015; Kwiatkowski et al., 2020) which may not allow a mechanistic understanding of specific processes because of intrinsic differences between the models. Large biases in the modeled oxygen distribution in the oceans have been attributed to the inability of models to correctly simulate the equatorial and off-equatorial zonal, subsurface currents (Cabr e et al., 2015; Duteil et al., 2014; Oschlies et al., 2018).

Previous studies show the existence of alternating zonal jets at different depths in all ocean basins (Eden, 2006; Maximenko et al., 2005, 2008; Nakano & Hasumi, 2005; Richards et al., 2006). The connection between the zonal jets and oxygen concentrations has been mostly explored in the Pacific and Atlantic oceans, where the jets are shown to modulate tracer fields by generating large-scale frontal regions in the deep ocean (Delpech et al., 2020) and enhancing meridional oxygen gradients in the OMZs so that mesoscale eddy mixing becomes an important supply mechanism (Brandt et al., 2012; L evy et al., 2022). Busecke et al. (2019) highlight the importance of correctly simulating the equatorial current system in the Pacific Ocean and how the OMZ is sensitive to the magnitude and structure of the Equatorial Undercurrent. In the Atlantic OMZs, eastward jets are known to be important conduits of oxygen as they connect the more oxygenated western part of the basins with the OMZs in the eastern boundaries (Brandt et al., 2008, 2010, 2012; Burmeister et al., 2019; Stramma et al., 2008). Consequently, the long-term variability of the jets may in turn affect oxygen concentrations in the OMZs (Czeschel et al., 2011, 2015). For a recent overview on the phenomenology and dynamics of zonal jets in the ocean the reader is referred to Cornillon et al. (2019) and Kamenkovich et al. (2019) and references therein.

Two large-scale OMZs exist in the Atlantic Ocean. They arise as a combination of the subtropical circulation, which limits the ventilation of the eastern, tropical portion of the gyres, and the mostly wind-driven Eastern Boundary Upwelling Systems (EBUS) (Karstensen et al., 2008), characterized by high biological productivity and, consequently, high levels of respiration and remineralization in the water column, thus further decreasing oxygen concentrations.

In the Eastern Tropical North Atlantic (ETNA), a number of observations and modeling studies suggest that the equatorial current system has a large impact on the supply of oxygen-rich waters from the western part of the basin into the eastern part, thereby modulating the oxygen content of the OMZs (Brandt et al., 2010; Duteil et al., 2014). In fact, the sensitivity of the equatorial current system to natural oscillations may be a strong modulator of oxygen concentrations in the North Atlantic OMZ (Brandt et al., 2021). Therefore, a correct representation of the OMZ and its evolution relies on accurate simulations of the equatorial and off-equatorial current system. The ETNA is also characterized by a shallow OMZ, located near the coast and with a distinct vertical structure that is not captured by model simulations with resolutions up to 0.1  (Duteil et al., 2014; Frenger et al., 2018; Thomsen et al., 2019).

The eastern tropical South Atlantic (ETSA) OMZ is located between the Equator and Angola-Benguela Frontal Zone (ABFZ) (Tchipalanga et al., 2018). The surface flow is characterized by the intermittent, southward Angola Current (Kopte et al., 2017), which transports water from the equatorial region along the coast until it meets the Benguela current, where the flow turns offshore forming the ABFZ (Monteiro et al., 2008). Oxygen concentrations in the OMZ core are lower than in the ETNA OMZ. This could be due to the geometry of the basin, with the

OMZ core more isolated from the influence of the South Atlantic zonal jets, thus not receiving as much oxygen. Local biogeochemical processes in the water column associated with longer residence times may also lead to more oxygen consumption and result in lower oxygen concentrations.

In this work, we compare two coupled physical-biogeochemical simulations of the Tropical Atlantic ocean at different horizontal resolutions to show that the increase in resolution (a) allows the emergence of more robust zonal jets at intermediate depths of 300–800 m which have a major impact on the overall structure of the North and South Atlantic OMZs by limiting their westward extent and supplying oxygen to the western edge of the OMZs and (b) provides a better representation of the coastal and shelf current system as well as a more robust eddying field at depth which effectively redistribute low oxygen values that originate from the productive eastern boundary upwelling regions.

2. Methods

We use version 1.1 of the Coastal and Regional Ocean Community Model (CROCO) <https://www.croco-ocean.org/> coupled with the biogeochemical model PISCES in order to investigate the sensitivity of the North and South Atlantic OMZs to the large-scale ocean circulation in a climatological sense. The aim is to obtain a realistic representation of the oxygen structure in the OMZs of the Atlantic Ocean and its sensitivity to the ocean circulation, in particular to the equatorial current system, so that the model can be used for more accurate predictions of the temporal evolution of the oxygen content in the basin.

We use initial conditions for the physical variables (Sea surface height, temperature, salinity and horizontal velocity) from 1 January 2003 from the version 3.3.1 of the SODA reanalysis product (Carton et al., 2018). Boundary conditions for the same variables are obtained each 5 days for the same year and were downloaded from the Asia-Pacific Data Research Center at http://apdrc.soest.hawaii.edu:80/dods/public_data/SODA/soda_3.3.1/. The year 2003 was chosen because it is considered a neutral year both in terms of the North Atlantic Oscillation (NAO) (Chassignet & Xu, 2017) and the Atlantic Meridional Mode (AMM). With neutral oceanic conditions, we used climatological wind stress and heat fluxes from COADS as surface forcing. Initial and boundary conditions for the biogeochemical variables were obtained from a climatological PISCES run (Aumont & Bopp, 2006).

The full model domain encompasses the whole Tropical Atlantic Ocean, from 19°S to 31°N and from 99° to 15°W. We used two horizontal resolutions, namely 1/10° and 1/30°, which roughly translates into a nominal horizontal grid size of 10 km (TATL10) and 3 km (TATL3), respectively.

Momentum advection is done with the third-order upstream biased scheme and tracer advection is done with the split and rotated third-order upstream biased advection scheme (RSUP3), where diffusion is split from advection and is represented by flow-dependent hyperdiffusion and isopycnal rotation (Marchesiello et al., 2009). This scheme is shown to be more effective in reducing spurious diapycnal tracer mixing in sigma-coordinate models. In this case, the tracer mixing coefficient is a function of the absolute value of the local velocity and the grid size as $B = \frac{1}{12}|U|(\Delta x)^3$, where U is the scale of the velocity field and Δx is the grid size. Therefore, the smaller grid size of TATL3 yields a smaller diffusivity coefficient which may favor the emergence of zonal jets at depth.

Starting from the initial conditions from the SODA reanalysis, the physical and biogeochemical model were spun up for 9 years with climatological surface forcing. Results shown in this study are from monthly and annual averages of the last 7 years (year 10 to year 16) of model run. Daily averages are used in the calculation of the anisotropy coefficient in Section 4. The degree of anisotropy, α , is defined as (Huang et al., 2007),

$$\alpha = \frac{\langle u'^2 \rangle - \langle v'^2 \rangle}{\langle u'^2 \rangle + \langle v'^2 \rangle}, \quad (1)$$

where u' and v' are the zonal and meridional velocity anomalies from the averaged values for the specific averaging period, and the operator $\langle \rangle$ indicates temporal averaging, which is done at 6, 12, 24, 36, 48, and 60 months. We calculate α for four subdomains which are representative of the western part of the basin adjacent to the OMZs, namely ETNA-West (36°W–23°W, 5°N–16°N), ETSA-West (30°W–10°W, 16°S–5°S), ETNA-OMZ (23°W–23°W, 5°N–16°N) and ETSA-OMZ (10°W–10°E, 16°S–5°S).

The isopycnic PV is calculated from the model output averaged between isopycnal surfaces as

$$q = \frac{1}{\rho_0}(\zeta + f) \frac{\Delta\rho}{H}, \quad (2)$$

where ζ is the relative vorticity, ρ is the potential density, both averages of the values on each layer, H is the layer thickness and $\Delta\rho$ the density difference between the layers. Layer 1 is defined as the one between the 25.8 and 26.6 isopycnal surfaces and layer 2 is the one between 26.6 and 27.4 isopycnal surfaces.

In order to contextualize our results with existing global simulations, we use the output of the Global Ocean Physics Reanalysis (<https://doi.org/10.48670/moi-00021>) and the Global Ocean Biogeochemistry Hindcast (<https://doi.org/10.48670/moi-00019>). Both products are available at the Copernicus Marine Center Service (CMEMS) at <https://marine.copernicus.eu>. The physical model has a nominal horizontal resolution of $1/12^\circ$ and is forced with daily atmospheric fields from ERA-interim. In addition, observations from sea level, *in-situ* vertical profiles of temperature and salinity, sea surface temperature and sea ice are assimilated into the model. The biogeochemical model output is interpolated into a $1/4^\circ$ global grid from an original $1/12^\circ$ horizontal resolution run. No data assimilation is performed in the biogeochemical model. We compare our 7-year climatological simulations with the average of the whole period of the CMEMS product (1993–2019 in this case). This is not a coupled physical-biogeochemical run, these two products were chosen because of the availability of the data on the same time range. The physical model used in the biogeochemical hindcast (the non-assimilative FREEGLORYS2V4 run) is not available on the CMEMS website. More details about these simulations may be found on their website.

2.1. Oxygen Budget

The oxygen budget in the model is a combination of physical and biological processes as follows

$$\frac{\partial O_2}{\partial t} = \left(\frac{\partial O_2}{\partial t} \right)_{Physics} + \left(\frac{\partial O_2}{\partial t} \right)_{Biology}, \quad (3)$$

where

$$\left(\frac{\partial O_2}{\partial t} \right)_{Physics} = - \underbrace{u_h \cdot \nabla O_2}_{Horizontal\ Advection} - \underbrace{w \frac{\partial O_2}{\partial z}}_{Vertical\ Advection} + \underbrace{\frac{\partial}{\partial z} \left(K_z \frac{\partial O_2}{\partial z} \right)}_{Vertical\ Mixing}, \quad (4)$$

where K_z is the mixing coefficient, u_h are the horizontal components of the velocity vector and w is the vertical velocity.

The effect of biological processes on the oxygen concentration in PISCES is computed as follows,

$$\left(\frac{\partial O_2}{\partial t} \right)_{Biology} = \underbrace{(R_{o:c}^1 + R_{o:c}^2)(\mu_{NO_3}^P P + \mu_{NO_3}^D D)}_{New\ Production} + \underbrace{R_{o:c}^1(\mu_{NH_4}^P P + \mu_{NH_4}^D D)}_{Regenerated\ Production} - \underbrace{\lambda_{DOC}^* f(O_2) DOC}_{Remineralization} - \underbrace{G^Z Z - G^M M}_{Respiration} - \underbrace{R_{o:c}^2 Nitrif.}_{Nitrification}. \quad (5)$$

Oxygen is produced during photosynthesis via new and regenerated production by diatoms (D) and nanophytoplankton (P) and consumed by dissolved organic matter (DOC) remineralization, respiration by small (Z) and large (M) zooplankton and nitrification. λ_{DOC}^* is the remineralization rate and $f(O_2)$ is a function that varies between 0 and 1 to represent oxic or anoxic remineralization, depending on local oxygen concentrations. Stoichiometric oxygen to carbon ratios during ammonium conversion into organic matter ($R_{o:c}^1$) and during nitrification ($R_{o:c}^2$) are set to 140:122 and 32:122, respectively. G^Z and G^M are functions for zooplankton and mesozooplankton grazing whose details may be found in Resplandy et al. (2011). More details about the model structure and parameterizations may be found in Aumont et al. (2003).

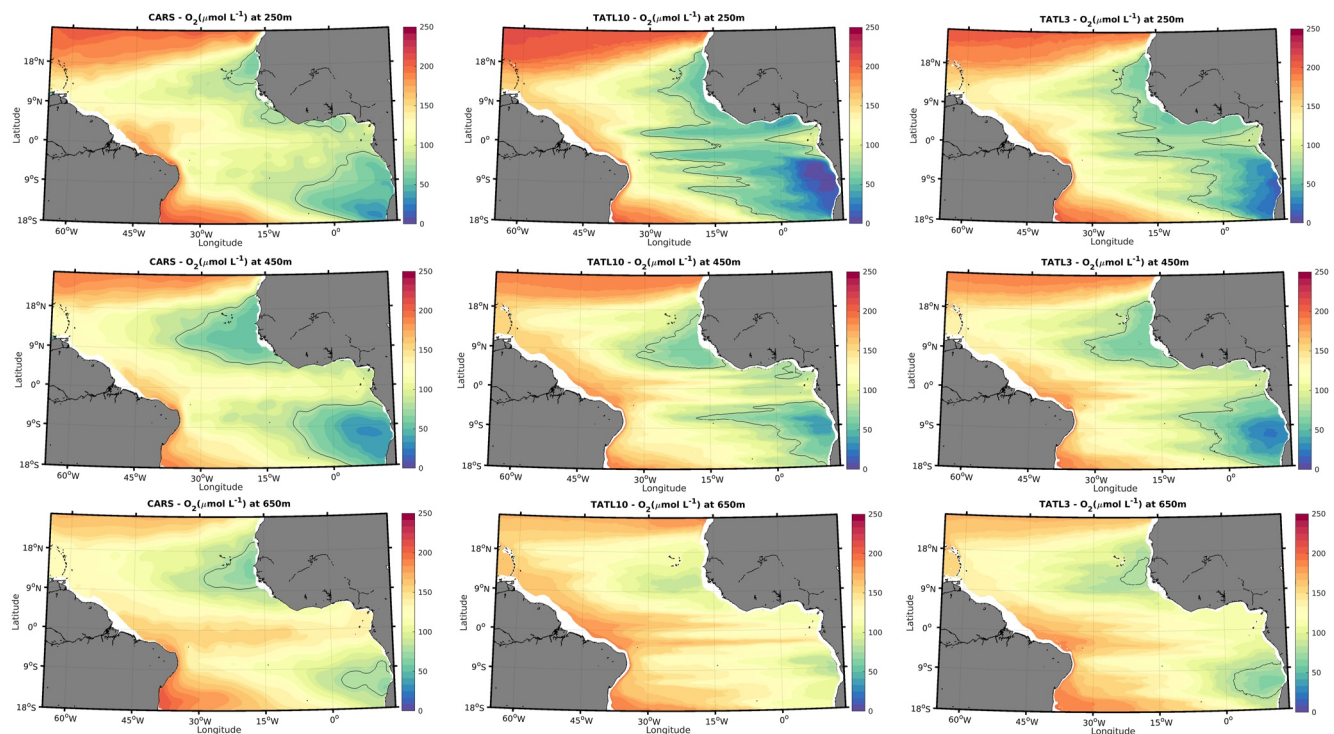


Figure 1. Horizontal maps of oxygen concentrations at 250, 450 and 650 m depths from the CARS climatology (left) and 7-year averages of TATL10 (middle) and TATL3 (right). Black lines show the $80 \mu\text{mol L}^{-1}$ oxygen concentration isoline.

3. Results

3.1. Horizontal Structure of Oxygen and Velocity Fields

Overall, both simulations capture the climatological structure of the surface circulation of the Tropical Atlantic. The 7-year averages of modeled surface velocities compare equally well with climatological averages obtained from surface drifters (Laurindo et al., 2017) (Figure A1) as the main large-scale features, namely the eastward-flowing North Equatorial Counter Current (NECC), the northern and southern branches of the westward-flowing South Equatorial Current (SEC) and the North Brazil Current and its retroflexion in the western part of the basin are correctly simulated.

A detailed model evaluation in terms of the horizontal and vertical tracer structure as compared to the CARS climatology is provided in the Appendix. The statistics required for the Taylor and target diagrams (Figures A2 and A3) are calculated from the regridded 7-year model averages to match the resolution of the climatology. Given the relatively low resolution of the climatology, these metrics serve to identify the ability of the models to simulate the large-scale, climatological structure of the tracers. Both simulations provide a relatively good skill in the North and South Atlantic OMZs, with some improvement in terms of correlation and bias in TATL3, particularly for nitrate and oxygen, with correlation coefficients larger than 0.8, which shows that the model is able to capture the correct range of variability and spatial patterns as compared to the CARS climatology (Figures A2 and A3). The improvement in TATL3 is also seen in the vertical transects shown in the next section and in the Appendix. We must keep in mind, however, that our “truth,” namely the CARS climatology, is a product created from the interpolation and extrapolation of sparse data. As such, it is also prone to errors, particularly in relatively sub-sampled regions such as the South Atlantic Ocean. This can be one of the reasons why the correlation between some of the model and climatology variables is relatively low at 650 m depth in the South Atlantic (Figure A2). A useful discussion on biogeochemical model evaluation is provided in Doney et al. (2009); Jolliff et al. (2009).

While both runs could be considered acceptable in terms of their climatological model skill, a detailed visual inspection of the oxygen distribution at specific depths reveals large differences both in terms of oxygen

concentration as well as the geometry of the OMZs. Figure 1 shows a comparison between the 7-year average of TATL10 and TATL3 and the CARS climatology at 250 m, 450 and 650 m depths. TATL3 is more similar to the CARS climatology than TATL10 both in terms of oxygen concentrations and the structure of the OMZs, as seen by the $80 \mu\text{mol L}^{-1}$ isoline which is assumed to be the limit of the OMZ. In TATL10, lower oxygen values at 250 m depth are advected much further west than in TATL3. The westward excursions of the $80 \mu\text{mol L}^{-1}$ isoline suggest a strong influence of alternating zonal jets in the equatorial/tropical region on oxygen concentrations, with westward jets advecting low oxygen waters and eastward jets advecting high oxygen waters given the large-scale zonal oxygen gradient. TATL10 also strongly underestimates oxygen concentrations in the ETSA region at 250 m with values as low as $10 \mu\text{mol L}^{-1}$ as opposed to TATL3 which is more similar to CARS at this depth. At 450 m depth, the impact of eastward equatorial currents is seen in both simulations as they effectively transport high oxygen waters and separate the two OMZs. At 650 m depth, the OMZ practically vanishes in TATL10 while TATL3 shows a structure more similar to the climatology.

At 450-m depth and below, the high oxygen concentrations in the western part of the basin, between 8°N and 18°N , persist in TATL10 as opposed to TATL3, which is more in line with the climatology. This suggests that eddying processes at depth, responsible for tracer redistribution, are not properly resolved by the 10-km resolution run which can have serious consequences for climate simulations unless these processes are adequately parameterized.

The impact of the zonal jets on the OMZ structure at these depths is shown in Figure 2 with the 7-year averaged zonal velocities and the OMZ boundary at 250, 450 and 650 m depths. At 250 m, westward jets extending all the way across the basin in TATL10 are responsible for the unrealistic westward extension of the OMZ. In TATL3 these jets become weaker on the eastern part of the basin with a reduced ability to advect low oxygen waters westward. In addition, the magnitude of the zonal jets in TATL3 is larger than in TATL10, particularly eastward jets. They not only supply oxygen-rich waters from the western part of the basin but also delimit the westward extent of the OMZ boundary as they weaken past that point both in the ETNA and the ETSA. Interestingly, the number of zonal jets increases in the North Atlantic in TATL3, particularly in the western part of the basin. The zonal jets located at around 9°N , 12°N , and 15°N seem to be particularly relevant for the ETNA OMZ. At 650 m the pattern is similar, with the zonal jets still robust in TATL3.

3.2. Vertical Structure

The meridional distribution of 7-year averaged oxygen concentrations at 23°W (Figures 3a–3c) shows two minima which correspond to the deep OMZs in each hemisphere. The northern minimum, as shown in the CARS climatology, is located at 11.5°N at 450 m depth with oxygen concentrations of $54.1 \mu\text{mol L}^{-1}$. The southern one is located at 7.0°S at 400 m depth with oxygen concentrations of $89.7 \mu\text{mol L}^{-1}$. Because of the geometry of the basin, 23°W is further away from the ETSA than from the ETNA. The climatological structure is better reproduced by TATL3, which shows the two minima at approximately the same latitudes and depths as in the CARS climatology, with slightly larger minimum oxygen concentrations, $66.1 \mu\text{mol L}^{-1}$ in the ETNA extension and $98.2 \mu\text{mol L}^{-1}$ in the ETSA extension. The OMZ is located within the limits of Central ($\sigma_{\theta} = 25.8 - -27.1 \text{ kg m}^{-3}$) and Antarctic Intermediate Waters ($\sigma_{\theta} = 27.1 - -32.15 \text{ kg m}^{-3}$), consistent with observations (Karstensen et al., 2008). Oxygen maxima are associated with the latitudinal positions of the intermediate eastward jets which seem to be responsible for the large-scale, meridional distribution of oxygen with a peak at around 2°S . Taylor and target diagrams (Figure A4) show that oxygen concentrations in TATL3 have the highest correlation (0.94) with the CARS climatology and the smaller bias and root mean square deviation.

The vertical structure of the zonal currents in the upper 300 m (Figures 3d and 3e) is well reproduced by both simulations when compared to previous observational work at the same longitude (Brandt et al., 2010, 2015; Burmeister et al., 2019), with the Equatorial Undercurrent (EUC) core at the Equator, the North Equatorial Countercurrent (NECC) from roughly 4°N to 10°N mainly in the upper 100 m with a narrow subsurface expression at 5°N , which corresponds to the North Equatorial Undercurrent (NEUC) whose stronger counterpart, the South Equatorial Undercurrent (SEUC), is seen at 4°S . The main difference between the two runs in the upper 300 m is a stronger branch of the NECC at 6°N in TATL3 than in TATL10. This branch, as well as a deeper eastward current at this latitude, is consistent with the observations of Burmeister et al. (2019) from February to March 2018, although it is not as pronounced in the zonal average obtained by Brandt et al. (2010); Brandt et al. (2015).

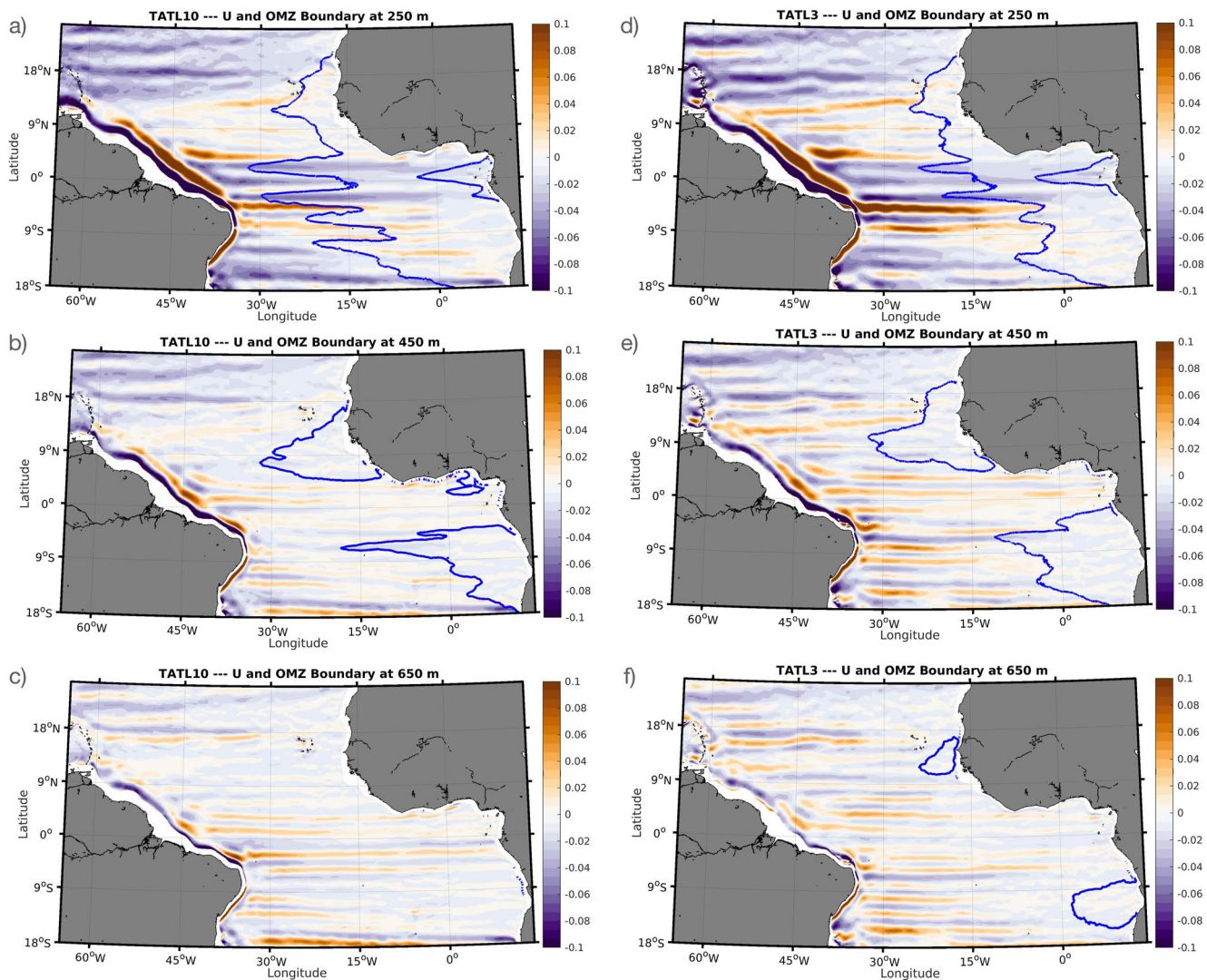


Figure 2. 7-year averages of the zonal velocities from TATL10 (left) and TATL3 (right) at 250, 450 and 650 m depths. Blue lines show the $80 \mu\text{mol L}^{-1}$ oxygen concentration isoline.

Below 300 m, more intense intermediate zonal jets in TATL3 than in TATL10 have important consequences for the supply of oxygen to the core of the OMZs, roughly between 350 and 800 m depth. Both runs show alternating jets whose wavelength is approximately 2.5° in latitude, consistent with observational and modeling estimates that show alternating zonal jets at mid-depth (Eden, 2006; Maximenko et al., 2005; Nakano & Hasumi, 2005; Richards et al., 2006). They reproduce the Northern and Southern Intermediate Countercurrents (NICC and SICC) at approximately 2°N and 2°S , respectively. The more robust jets in TATL3 suggest that eddy-driven processes, not fully resolved at 10 km horizontal resolution, are important in their formation and maintenance, as suggested by previous works (Eden, 2006; Lévy et al., 2010; Nakano & Hasumi, 2005).

Both TATL10 and TATL3 show two oxygen minima equidistant from the Equator at approximately 2.5°S and 2.5°N at around 250 m depth. These are shallower than the deep OMZs in each hemisphere and while they are not very evident in the CARS climatology, these features are consistent with the observations of Brandt et al. (2010); Brandt et al. (2012) which show that these minima are due to the westward-flowing northern and equatorial branches of the South Equatorial Current. These are stronger in TATL10, which explains the lower oxygen concentrations (around $60 \mu\text{mol L}^{-1}$, as opposed to $83 \mu\text{mol L}^{-1}$ in TATL3) at approximately the same locations, as these westward currents advect low-oxygen waters from the OMZs, as discussed previously (see also Figure 2). A zonal transect of the zonal velocity at 6.4°N shows larger values from 450 m down to 1,000 m in TATL3 than in

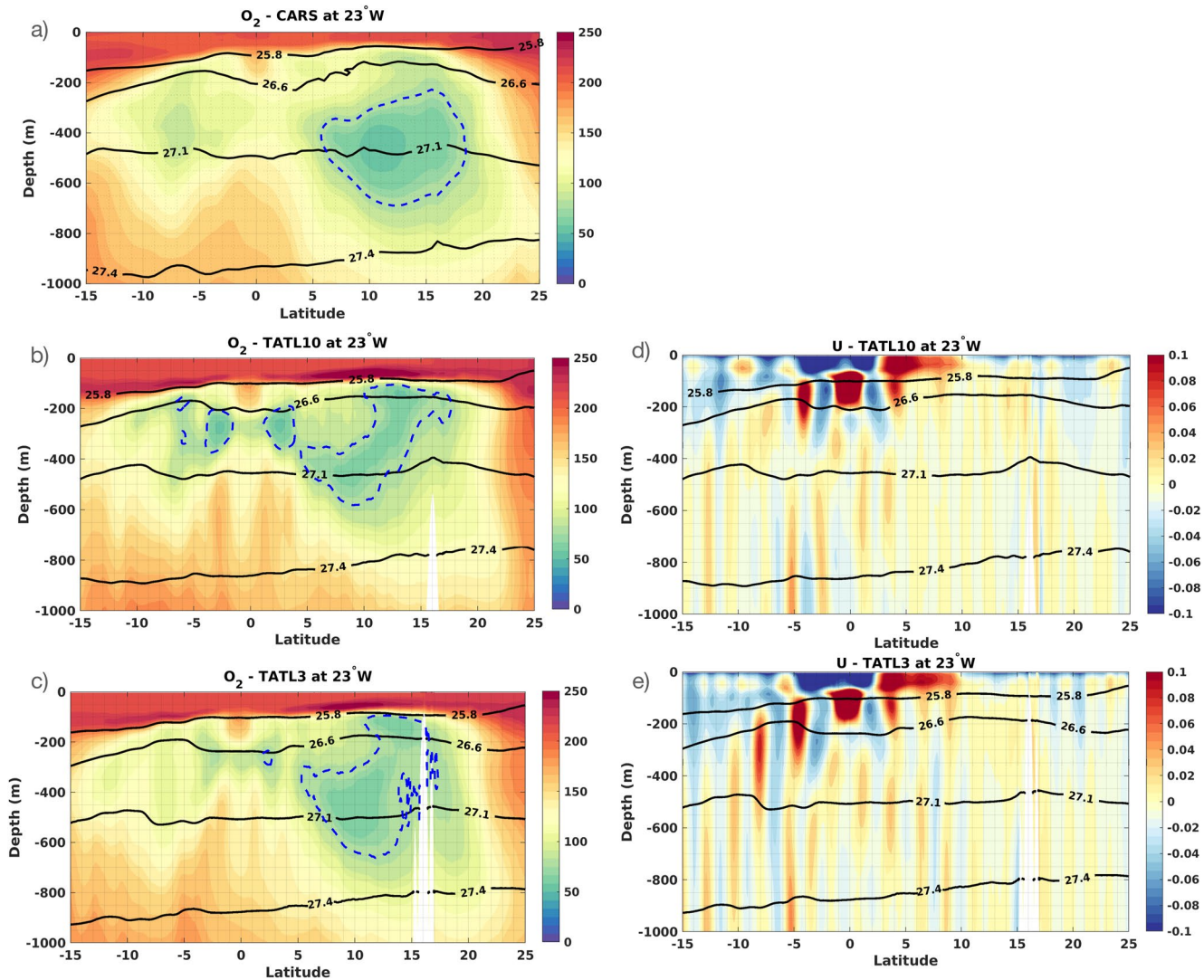


Figure 3. Meridional transects of climatological oxygen concentrations from (a) CARS and 7-year averages from (b) TATL10 and (c) TATL3 at 23°W. Right panel shows the 7-year averaged zonal velocities for (d) TATL10 and (e) TATL3 at the same longitude. Isopycnal surfaces 25.8, 26.6, and 27.1 kg m⁻³ are shown as black lines.

TATL10 (Figure A5), with a corresponding eastward retraction of the 80 μmol L⁻¹ oxygen concentration isoline. A similar pattern is seen at other latitudes (not shown).

The ETNA is also characterized by a shallow OMZ just below the mixed layer, between 60 and 200 m deep, which arises as a combination of remote, physical drivers, namely, transport of SACW by the boundary current system and local organic matter remineralization due to biological productivity in the area (Karstensen et al., 2008; Thomsen et al., 2019). Figure 3 shows that the shallow ETNA OMZ is captured in both runs. Oxygen concentrations in the ETNA OMZ at 23°W in TATL10 are around 58.3 μmol L⁻¹ reaching from 130 m depth at 13.3°N down to 510 m at 8.8°N. In TATL3 the shallow ETNA OMZ at the same longitude is located roughly at 150 m depth and the deeper, more pronounced minimum at around 10.5°N, at 468 m depth with oxygen concentrations of 62.8 μmol L⁻¹. The zonal oxygen distribution at 11°N (Figure A6), the latitude at which the ETNA OMZ is more pronounced as seen in Figure 3, shows that the hypoxic layer reaches 36°W with minimum concentrations of approximately 50 μmol L⁻¹ along the σ_θ isoline of 27.1 kg m⁻³, consistent with observational estimates (Karstensen et al., 2008). The limitations of TATL10 in reproducing a realistic OMZ structure are clear in the zonal transect as the structure of the deeper OMZ is shallower and more confined to the coast than in the

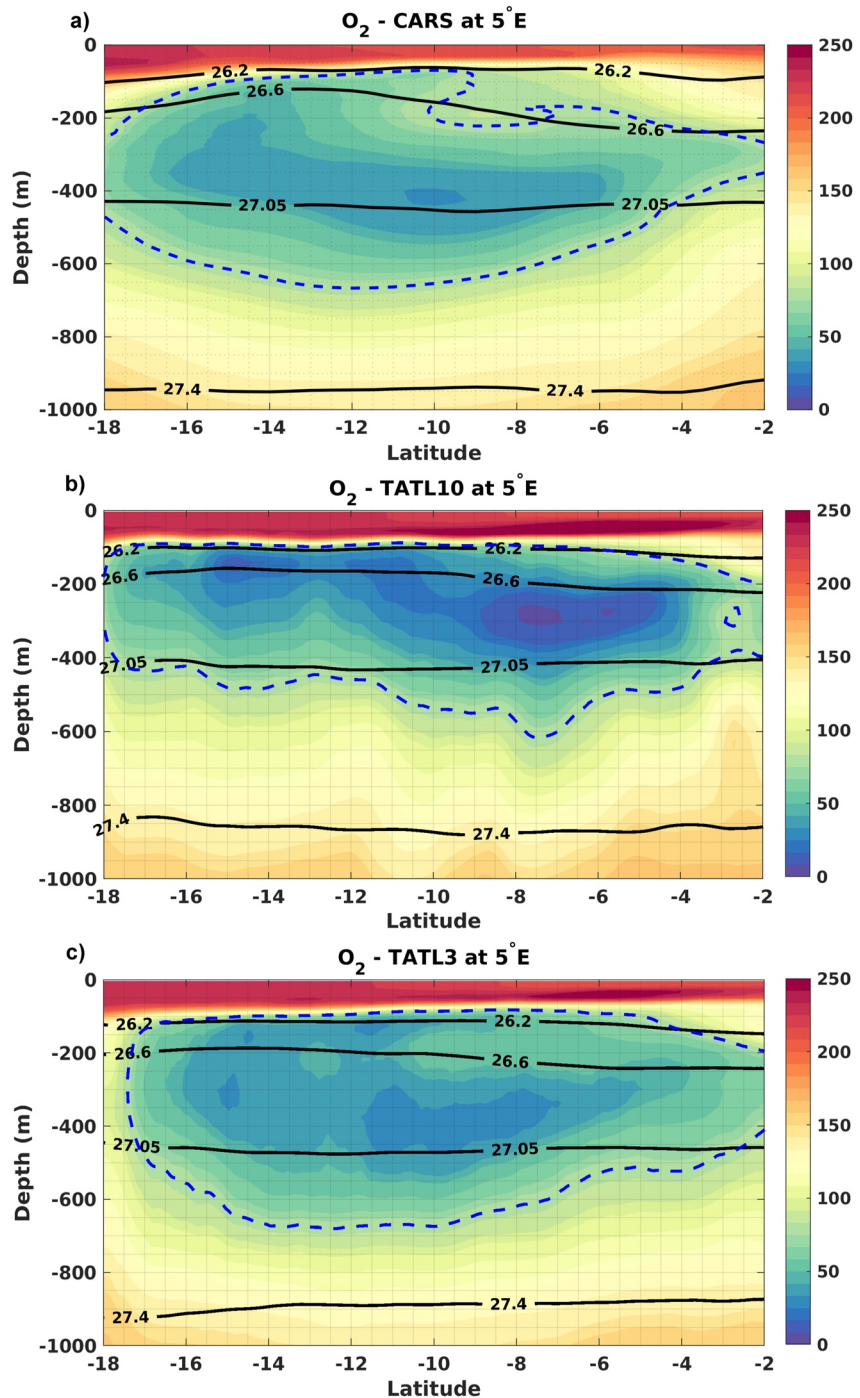


Figure 4. Meridional transect of climatological oxygen concentrations from CARS (top) and 7-year averages from TATL10 (middle) and TATL3 (bottom) at 5°E. Isopycnal surfaces 26.2, 26.6, and 27.05 kg m^{-3} are shown as black lines.

climatology. This results in a lower correlation (0.82 vs. 0.93 in TATL3) and a larger normalized bias for oxygen concentrations, as seen in the Taylor and target diagrams in Figure A4.

In the South Atlantic, a meridional transect at 5°E, within the Angola Gyre (Gordon & Bosley, 1991) is shown in Figure 4. This transect is characterized by a wider OMZ south of 12°S, from 100 to 400 m, and a deeper OMZ north of 12°S. These features are seen in observations from a cruise in 1995, as shown by Karstensen et al. (2008) (their Figure 3). Only TATL3 is able to reproduce the recirculation of the Angola Gyre, which is responsible for

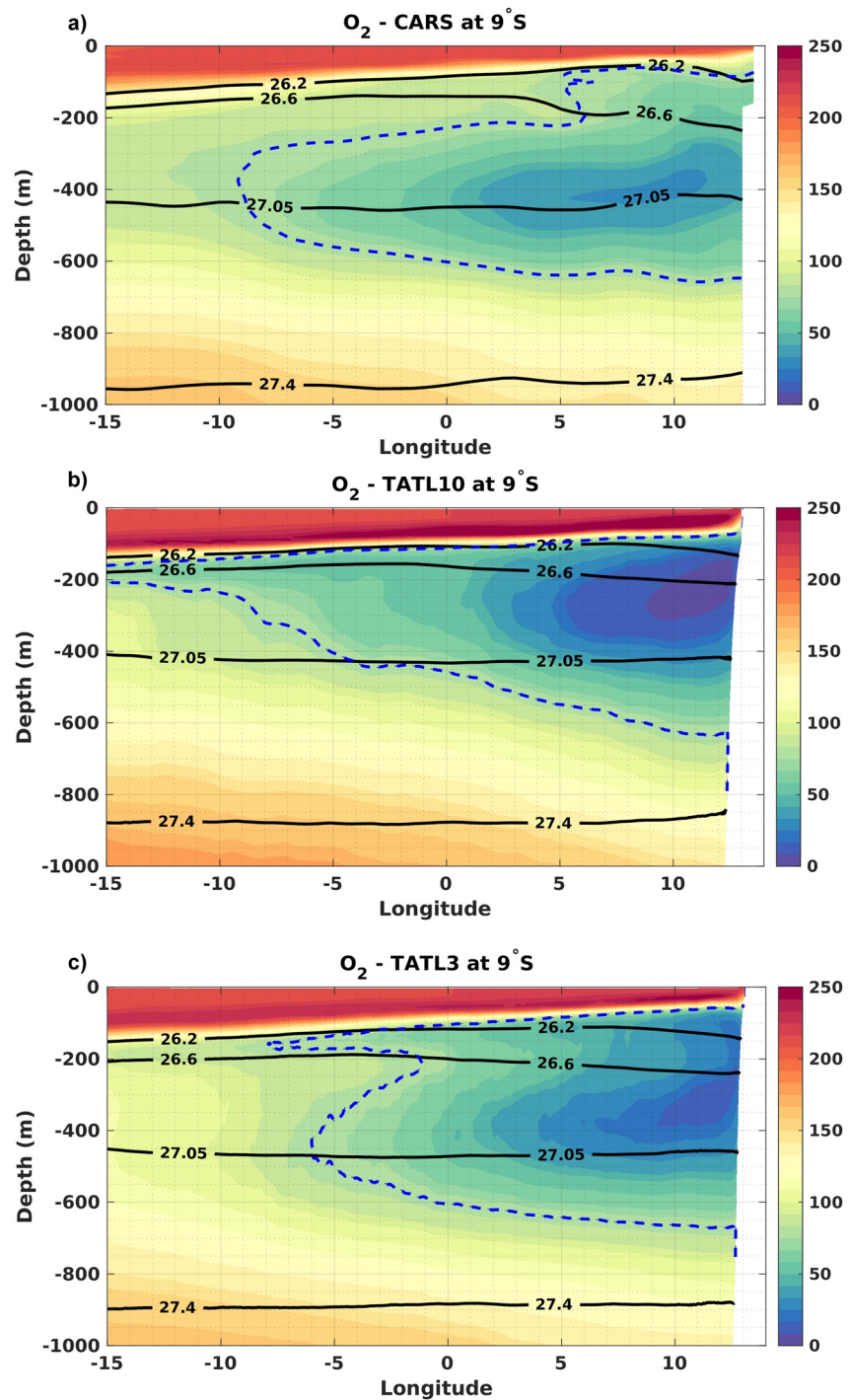


Figure 5. Zonal transect of climatological oxygen concentrations from CARS (top) and 7-year averages from TATL10 (middle) and TATL3 (bottom) at 9°S. Isopycnal surfaces 26.2, 26.6, and 27.05 kg m^{-3} are shown as black lines.

the OMZ structure south of 12°S. The correlation between the modeled oxygen and the CARS climatology for this section is 0.96 in TATL3 against 0.85 in TATL10 (Figure A4).

A zonal transect at the core of the ETSA OMZ at 9°S from CARS shows the deep OMZ at around 400 m depth with oxygen concentrations as low as $32.5 \mu\text{mol L}^{-1}$ between 5°E and 10°E, just above the 27.05 kg m^{-3} isopycnal (Figure 5). The climatology does not show a clear shallow OMZ near the coast as in the ETNA, which is likely due to the lack of observations. The deep OMZ is located between the 26.6 and 27.05 kg m^{-3} isopycnals. TATL3

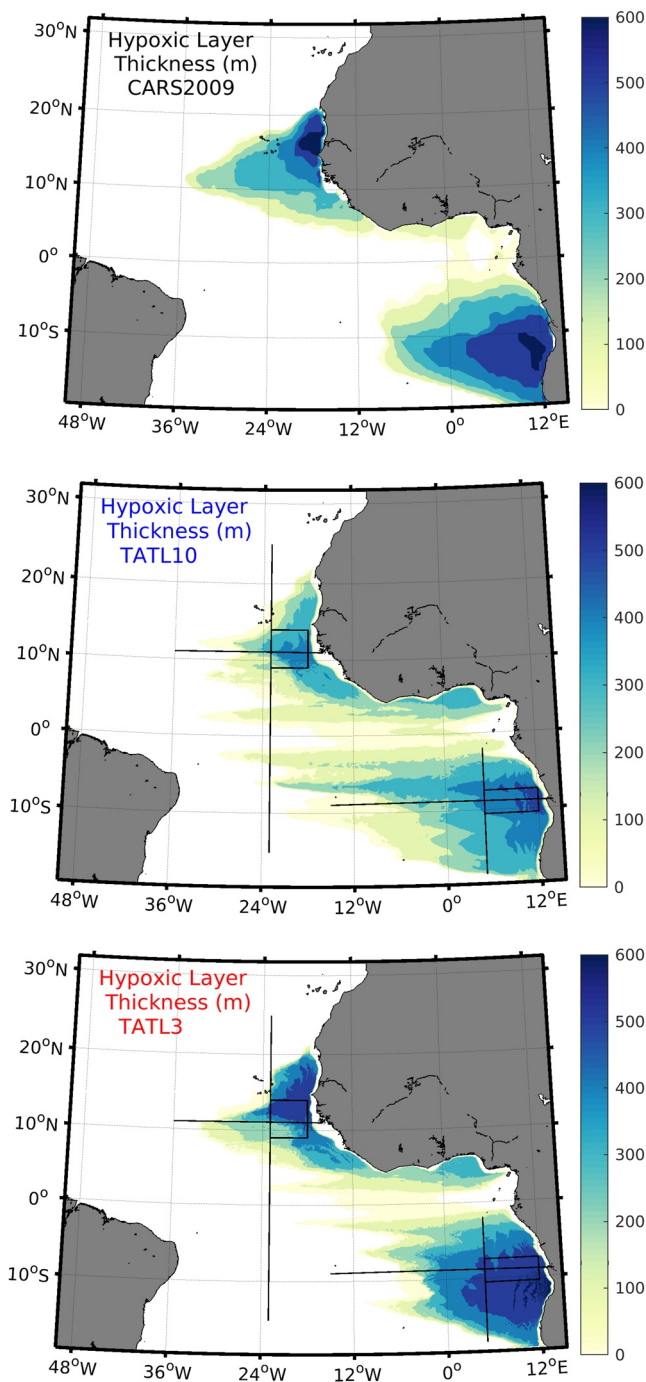


Figure 6. Thickness of the hypoxic layer, here defined as the layer which contains oxygen concentrations below $80 \mu\text{mol L}^{-1}$. Black lines highlight the sections at 23°W , 5°E , 9°S , and 11°N . The squares are the regions in ETNA and ETSA where the box-averaged oxygen budget terms are calculated (see Figure 11).

shows the deep OMZ at the correct depth, with a broader core as compared to the climatology, and lower oxygen concentrations ($19.1 \mu\text{mol L}^{-1}$ at around 350 m depth) than in the climatology. The zonal extent of the OMZ is also more similar to the climatology in TATL3 than in TATL10, as confirmed by the Taylor and target diagrams in Figure A4.

Figure 5 suggests that the source of low oxygen waters is the shelf region near the EBUS which is then diffused by coastal and shelf currents/undercurrents as well as the deeper circulation. Because these are not adequately resolved in TATL10, the low oxygen waters tend to be more confined near the source region. TATL3, on the other hand, seems to be more effective in simulating the mechanisms responsible for the diffusion of low oxygen waters, therefore providing a more realistic representation of the OMZ structure.

The relatively low horizontal resolution of TATL10 may not be sufficient to correctly simulate coastal and shelf processes that influence oxygen distribution, such as the dynamics of the poleward undercurrent and the formation of coastal eddies. Also, the low resolution of the wind stress forcing, which was deliberately used both in TATL10 and TATL3, may not generate the wind stress curl near the coast which is an important local vorticity source. Nevertheless, TATL3 is overall consistently better than TATL10 thus highlighting the importance of high horizontal resolution on a basin-scale simulation for a correct representation of the OMZ both in ETSA and ETNA.

3.3. Impact of the Jets on the OMZ Structure

From Figures 1 and 2, we see that westward velocities in the equatorial region tend to advect low-oxygen waters from the eastern boundary. These currents are similarly reproduced in both runs (Figure 3), but seem to have a stronger influence on the structure of the OMZs in TATL10. This is clearly seen when we compare the average hypoxic layer of each model run, defined as the thickness of the water column that comprises oxygen concentrations smaller than $80 \mu\text{mol L}^{-1}$, to the CARS climatology (Figure 6). The unrealistic westward extend of the hypoxic layer in TATL10 is primarily driven by the westward currents that flank the eastward-flowing EUC. In TATL3, the effect of these currents is counteracted by increased eastward velocities. TATL3 shows a much better agreement with the CARS climatology than TATL10 in terms of the structure and thickness of the Atlantic hypoxic layer. Despite the clear differences in the structure of the OMZs in the different runs, their averaged volume is surprisingly similar to the one from the climatology, as seen in Table 1. These values are consistent with the estimates of Karstensen et al. (2008), who used a threshold of $90 \mu\text{mol L}^{-1}$ for their calculation. The thinning of the OMZs in TATL10 is compensated by a larger areal extent induced by the westward zonal currents. Therefore, metrics such as the volume of the OMZs should not be presented without an examination of the horizontal and vertical structure as seemingly correct numbers may be misleading.

The asymmetry between the effect of westward and eastward jets in the different runs occurs because the former are associated with more homogenous potential vorticity (PV) tongues while the latter are associated with more intense PV gradients (Assene et al., 2020; Delpech et al., 2020). Figure 7

shows that the westward jets, associated with homogenized PV, are more pronounced in layer 1, which is equally reproduced in both runs, as shown by the zonal transport stream function in layer 1, meridionally integrated at 15°W (Figure 8a). Homogenous PV waters, associated with the shallow OMZ in the eastern part of the basin, are advected westwards. Eastward jets, associated with higher oxygen concentrations and more intense PV gradients,

Table 1
Volume of Hypoxic Waters (m^3)

Source	ETNA	ETSA
CARS	7.82×10^{14}	1.25×10^{15}
TATL10	8.12×10^{14}	1.26×10^{15}
TATL3	8.18×10^{14}	1.25×10^{15}

are stronger in TATL3 in both layers, thus effectively counteracting the westward advection of homogenized PV from the east. The inability of TATL10 in simulating the intermediate jets causes the horizontal stretching of the shallow OMZ and distorts its overall structure as shown in Figure 6.

The larger westward volume transport in layer 2, which contains the core of the OMZs, in TATL3 is confirmed by the calculation of the meridionally integrated zonal transport stream function (Figure 8b). The meridional integration started at around 9°S, where both velocities were near zero. Eastward zonal jet transport peaks are seen at around 4°N, 7°N, and 9°N, which is approximately the latitude of the intermediate jets in the layer-averaged zonal velocity, zonal transport and also in Figure 3.

3.4. Oxygen Budget

Monthly averages of the oxygen budget terms were saved for model years 13–16 (see Section 2.1). The 4-year averages of each term at 26°W, the western limb of the ETNA, shows that physical and biological processes largely balance each other out in the upper 200 m (Figure 9). This is true both for TATL3 and TATL10, with specific differences that are related to the impact of horizontal resolution on primary production and upper ocean dynamics which are out of the scope of this study. Between 200 and 800 m physical processes are responsible for oxygen supply, with the advection terms being larger in TATL3 than in TATL10, which is a consequence of the stronger intermediate eastward jets in TATL3. Vertical mixing is important for oxygen supply below the mixed layer, which makes it relevant for the oxygen balance in the shallow OMZ on short time-scales and for the deep OMZ in longer time-scales as it diffuses below the thermocline.

At 10°W, roughly the westward limb of the ETSA OMZ, the oxygen budget below 200 m is still dominated by advection as seen in Figure 10. It is largely positive in TATL3, particularly between 5°S and 12°S, and largely negative in TATL10. The increased oxygen supply at depth on the western edge of the ETSA OMZ in TATL3

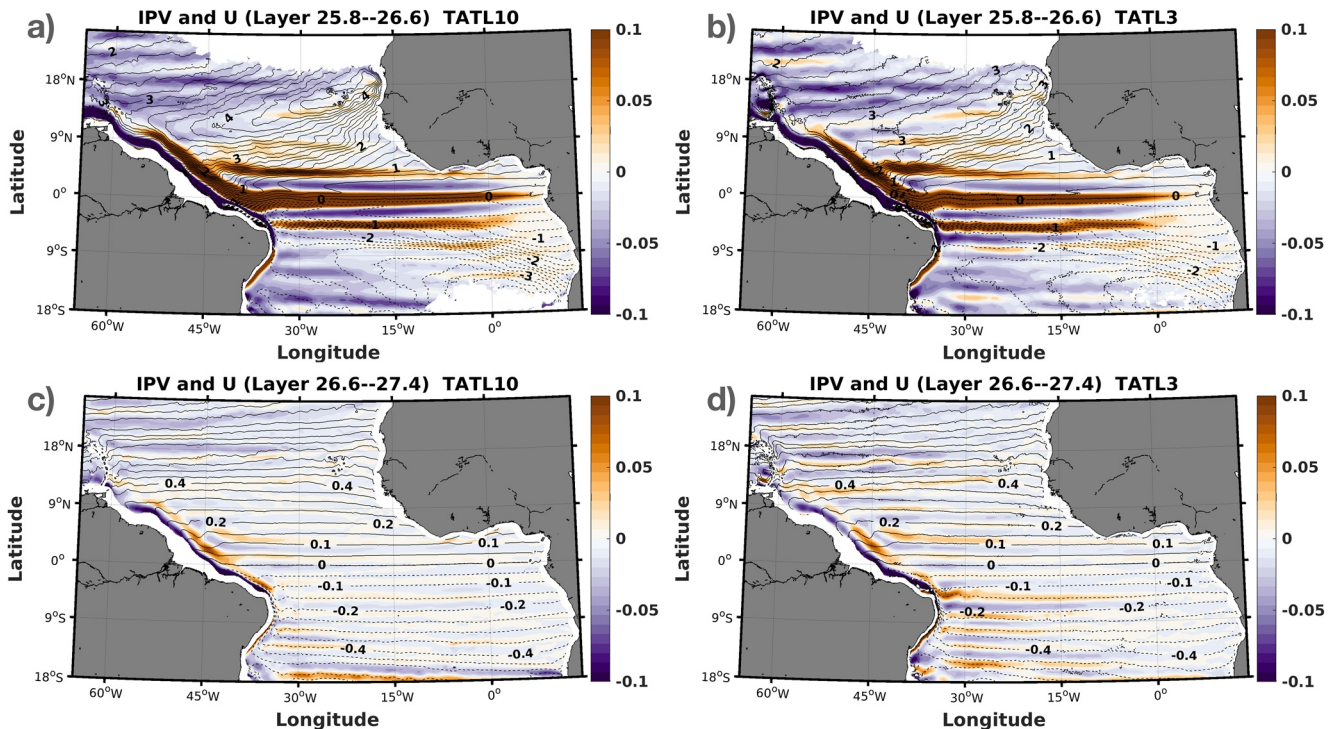


Figure 7. Contours of isopycnal potential vorticity ($\times 10^{-10} s^{-1} m^{-1}$) calculated from 7-year averages of the model runs for layer 1 (density classes 25.8 and 26.6 $kg m^{-3}$) and layer 2 (density classes 26.6 and 27.4 $kg m^{-3}$). Averaged zonal velocities between isopycnal surfaces are shown in color. For layer 1, the PV contour interval is $2 \times 10^{-11} s^{-1} m^{-1}$, for layer 2 the PV contour interval is $5 \times 10^{-12} s^{-1} m^{-1}$.

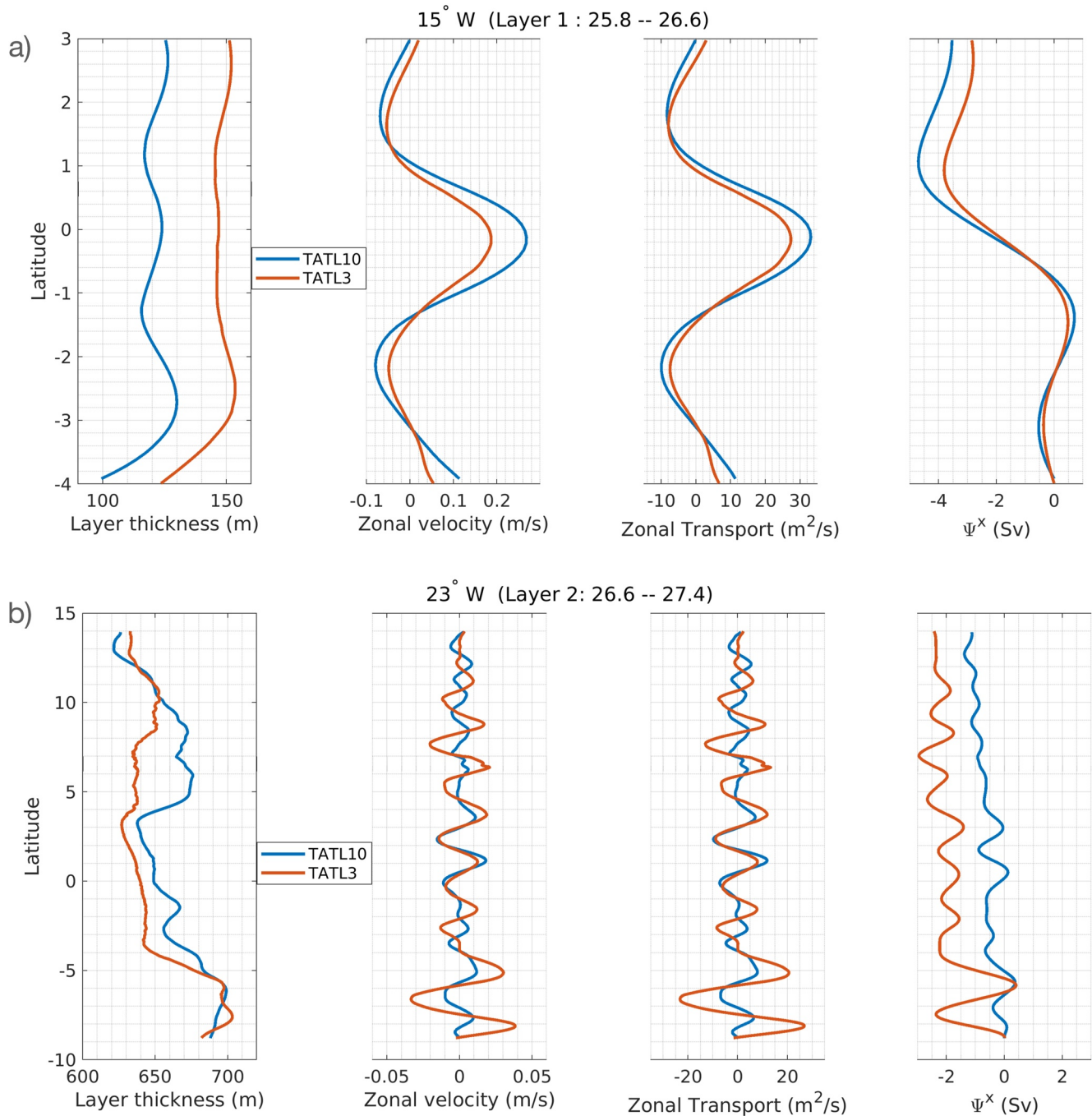


Figure 8. Layer thickness, zonal velocity, zonal transport and the meridionally-integrated zonal transport stream function for (a) layer 1 at 15°W and (b) for layer 2 at 23°W.

results in a more realistic OMZ structure as seen in Figures 1 and 6. The box-average at the core of the ETSA OMZ (10.5°S–7.5°S; 5°W–12°E) shows that biological consumption causes a deficit in the oxygen budget from 150 m down 400 m in TATL3. As it decreases with depth, advection and mixing are able to balance it between 400 and 700 m depth, the core of the OMZ in TATL3. Vertical mixing is a small, but positive contribution to the oxygen supply to the region from roughly 200 m down to 500 m in TATL3, and from 200 m down to 450 m in TATL10, but with a smaller magnitude. While the magnitude of vertical mixing is relatively small, the positive contributions show that it may be an important component of the oxygen budget over long time-scales (Lévy et al., 2022).

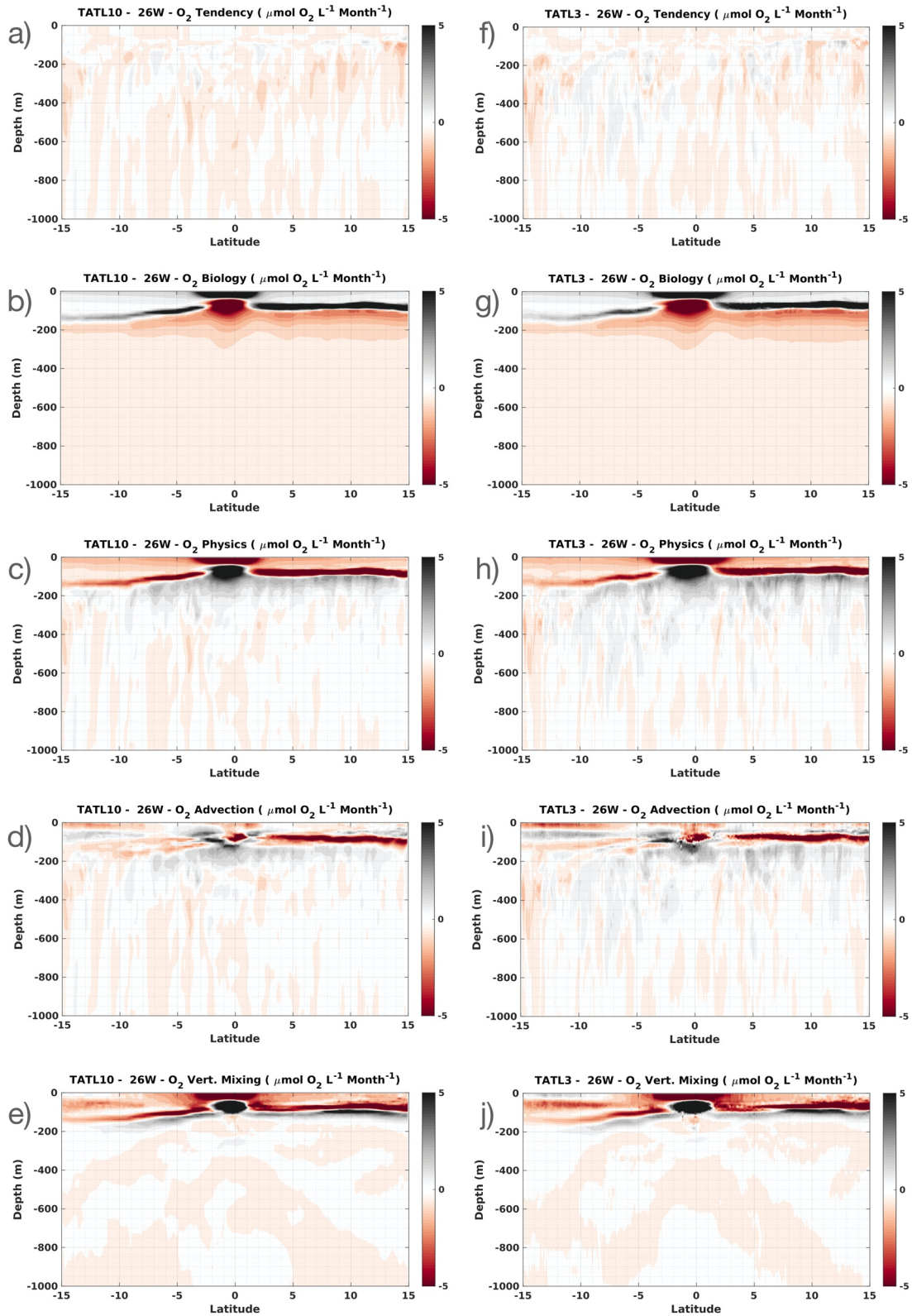


Figure 9. Four-year (Model years 13–16) averaged oxygen budget terms at 26°W for TATL10 (left) and TATL3 (right).

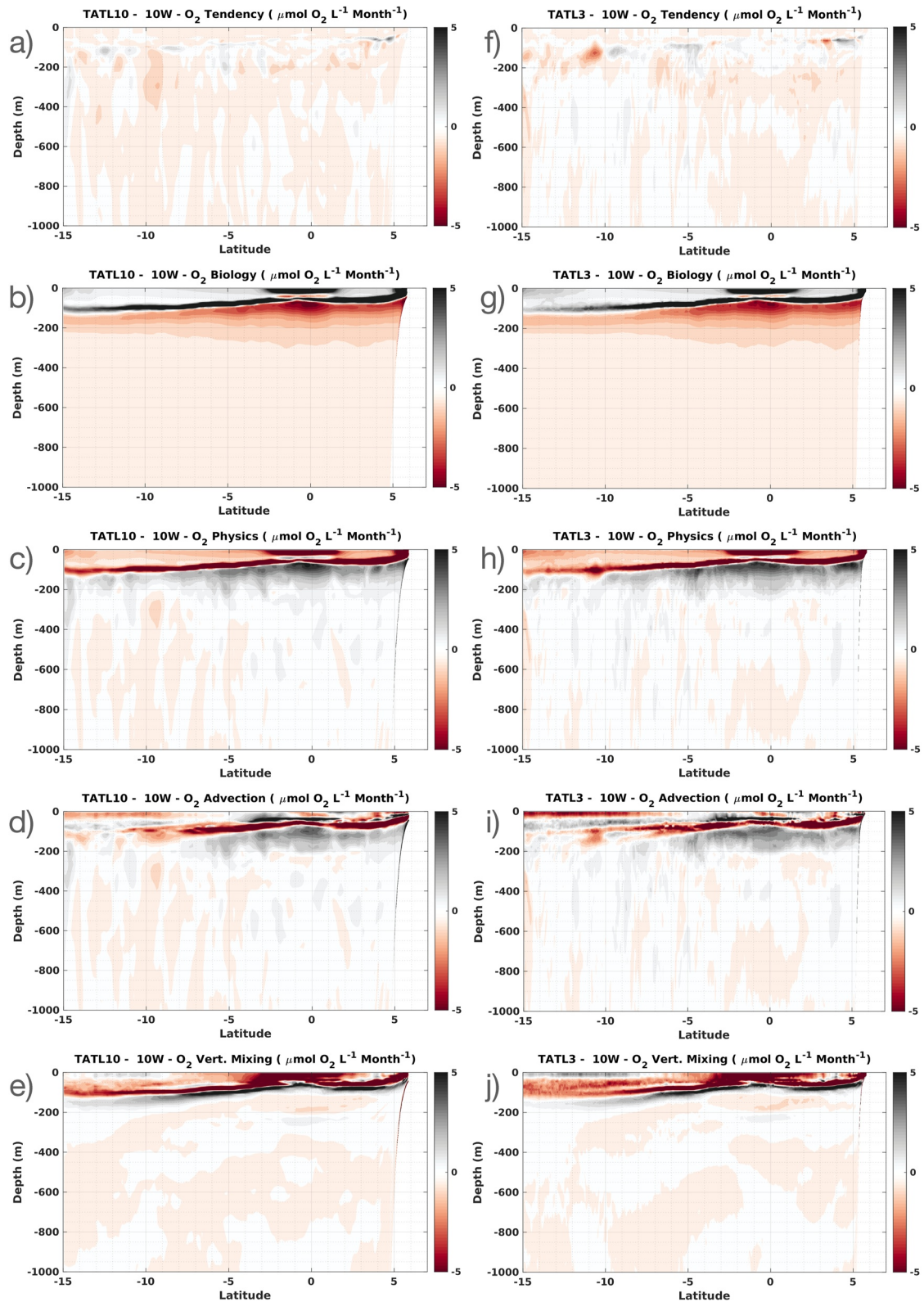


Figure 10. Figure-year (Model years 13–16) averaged oxygen budget terms at 10°W for TATL10 (left) and TATL3 (right).

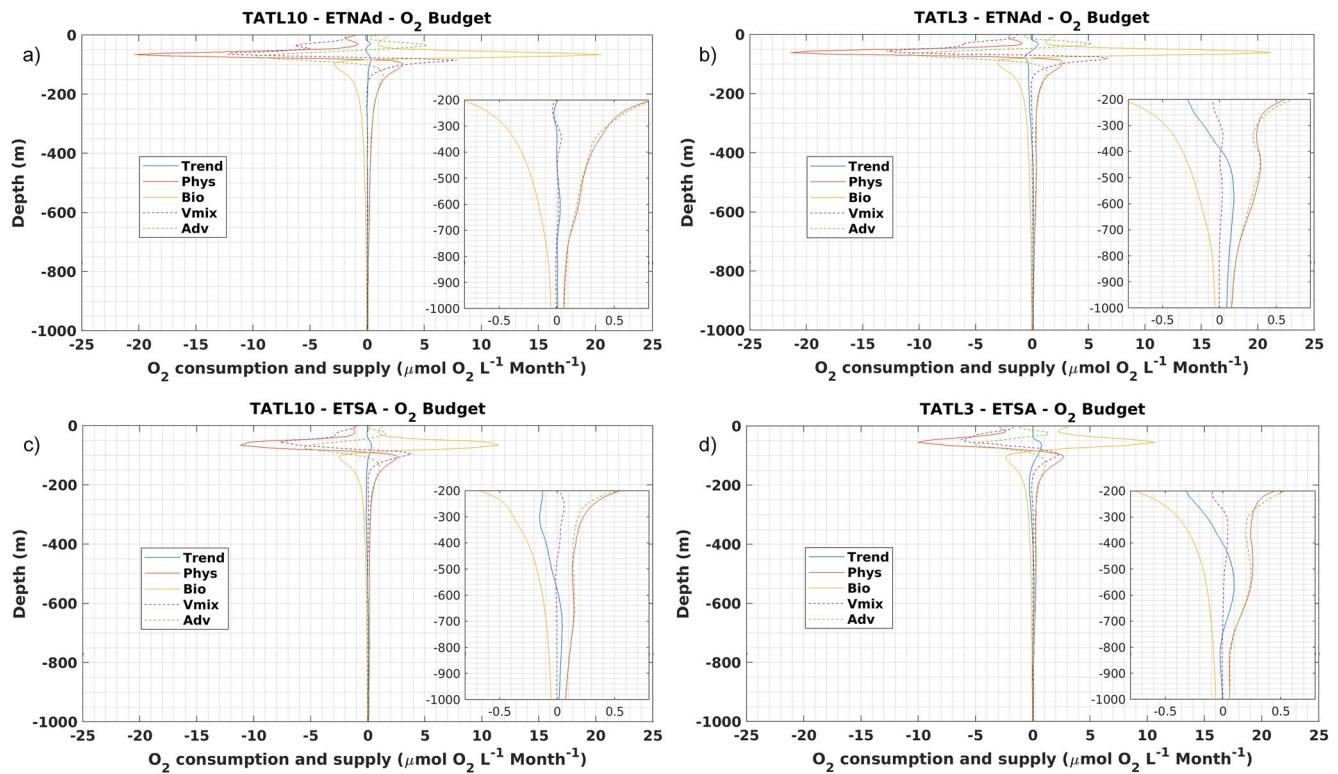


Figure 11. (a, b) Box-averaged oxygen budget terms in the deep ETNA OMZ region (9°N – 14°N and from 23°W to 18°W). (c, d) Box-averaged oxygen budget terms in the ETSA OMZ region (10.5°S – 7.5°S ; 5°W – 12°E).

A box average of the budget terms within the deep ETNA OMZ (9°N – 14°N ; 23°W – 18°W) illustrates the importance of advection in supplying oxygen to the OMZ core region. As seen in Figures 11a and 11b, below 380 m the supply of oxygen is largely dominated by advection, whose values are larger in TATL3 than in TATL10 between 350 and 700 m. The averaged biological consumption is relatively similar in both runs, $-3.09 \mu\text{mol L}^{-1} \text{ Year}^{-1}$ in TATL10 and $-3.28 \mu\text{mol L}^{-1} \text{ Year}^{-1}$ in TATL3. These values are comparable to the estimate of Karstensen et al. (2008) for a similar region, namely $-4.1 \mu\text{mol kg}^{-1} \text{ Year}^{-1}$. Admittedly, four years is a relatively short time to obtain a balanced budget, however, our results highlight the different impact of the advection terms in the oxygen budget in the two climatological runs.

4. Eddy-Driven Oxygen Supply

As shown by Hahn et al. (2014), the meridional eddy oxygen flux is also important in the OMZ. We calculated the eddy-driven meridional oxygen flux at 23°W (Figure 12) using the 7-year mean and deviations from that mean based on monthly values of the oxygen concentration and meridional velocities. The calculation was performed along isopycnals and the values were re-gridded onto depth coordinates. Values from both runs are consistent with those estimated by Hahn et al. (2014) using the diffusive flux parameterization (Figure 8 in their study) but TATL3 provides a more realistic representation of these fluxes as compared to the observational estimates. Specifically, we note the positive (northward) oxygen flux between 400 and 700 m near the ETNA boundary, between 4°N and 10°N , which drops to zero and becomes negative at the core of the ETNA OMZ.

To have a better idea of the importance of zonal versus meridional eddy velocities in and out of the OMZs, we calculate the degree of anisotropy α (Figure 13) (See Section 2). In the ETNA, there is a noticeable decrease in α from the western part into the OMZ, which suggests that meridional anomalies become more relevant in the OMZ. In the ETSA, the west-east decrease in α is not as pronounced as in the ETNA. It decreases in TATL3 when compared to TATL10, showing a more isotropic eddy field. Overall, the eddy flow at depth tends to be more isotropic than at 15 m, but even after removing the mean currents, where the zonal dominance is overwhelming, there is a slight anisotropy in the upper ocean favoring zonal currents. We note that our α values are

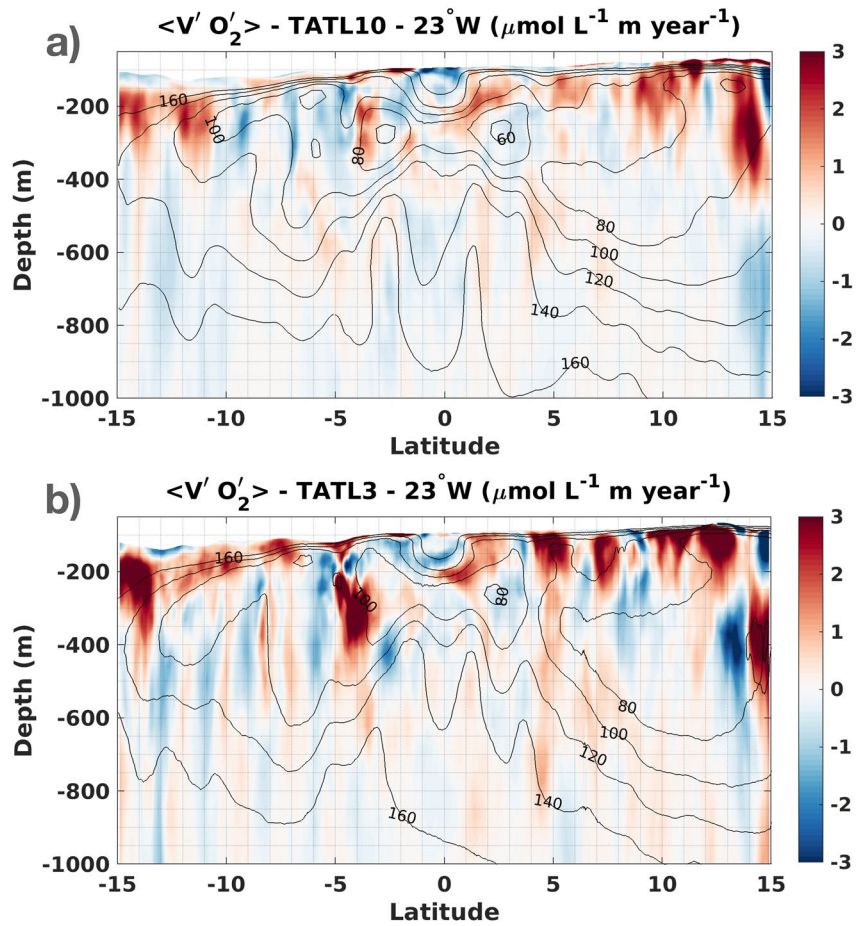


Figure 12. Seven-year average of the meridional eddy oxygen flux calculated from monthly averages of meridional velocities and oxygen concentrations. The calculation was performed on isopycnal surfaces and re-mapped onto depth coordinates.

relatively lower when compared to the ones from Huang et al. (2007), who calculated α for the Pacific ocean. This is probably because they used monthly means while we use daily means, which contain more variability in both components.

The increased eddying velocities in TATL3 yield larger eddy diffusivities than in TATL10 with large values usually associated with the location of the eastward zonal jets (Figure 14). Eddy diffusivities are estimated using the formulation of Eden and Greatbatch (2008).

$$\kappa = \sqrt{\frac{U_e^3}{2\beta}}, \quad (6)$$

where U_e is the r.m.s. eddy velocity and β is the meridional gradient of the Coriolis parameter. U_e is estimated with the averaged velocities between the 26.6 and 27.4 kg m⁻³ isopycnals as it is representative of the OMZs core regions. The magnitude of κ values is consistent with in-situ estimates based on tracer release experiments in the North Atlantic OMZ (Banyte et al., 2013). The increased values within the jets and the OMZs show that the high resolution run is more capable of redistributing tracers horizontally in intermediate layers than the low resolution run. This seems to be an essential for the correct simulation of the vertical structure of the OMZs.

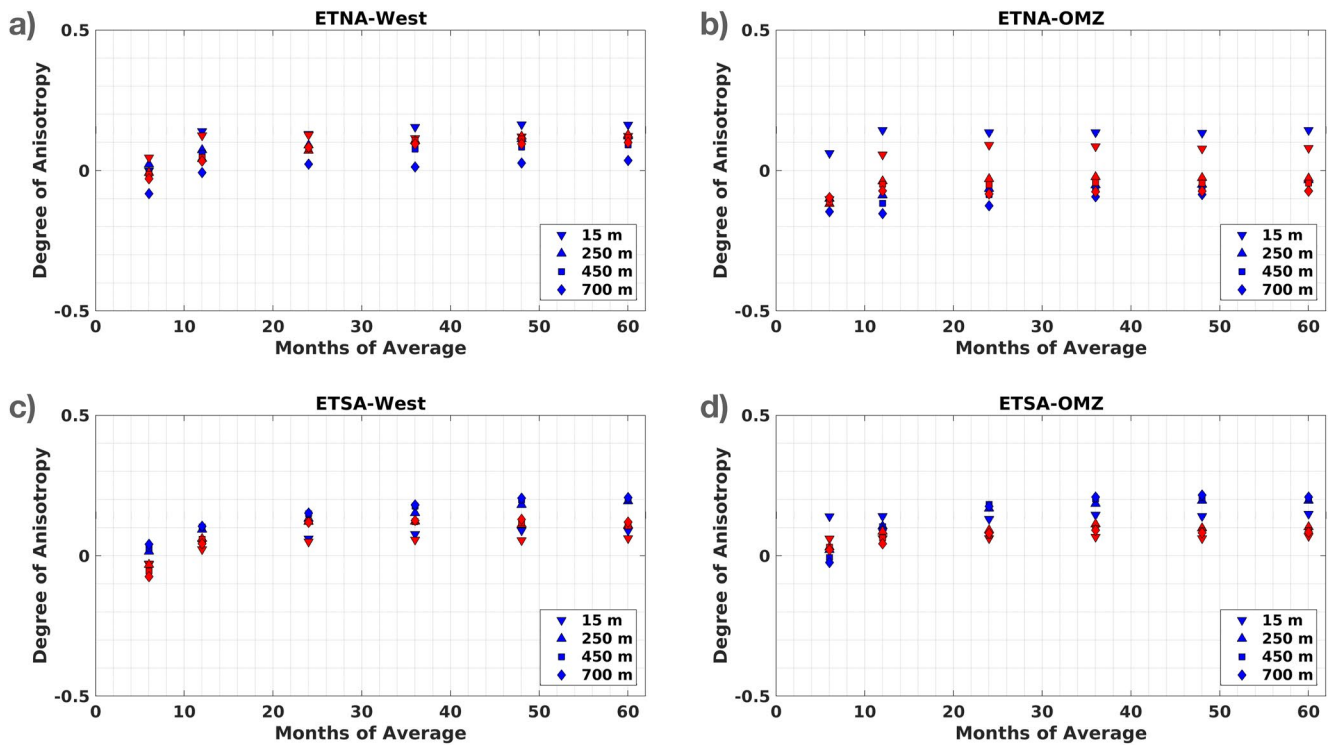


Figure 13. Degree of anisotropy (α) calculated from daily averages of 5 years of model run from TATL10 (blue) and TATL3 (red). α was calculated at different depths and for different time-averaging periods, namely 6, 12, 24, 36, 48, and 60 months.

5. How Does a Global Model Reproduce the Atlantic Zonal Jets and OMZs?

Variables from the CMEMS model are included in the Taylor and target diagrams shown in Figures A2–A4. The physical model from CMEMS has a better skill in simulating the climatological temperature and salinity structure than TATL3 and TATL10 as compared to CARS, particularly at depth. This is due to more realistic forcing and the data assimilation of physical variables. Nevertheless, some fundamental issues still remain as the relatively low horizontal resolution precludes the formation of robust, intermediate zonal jets away from the equatorial region, as seen in the average of the zonal velocity at 23°W. The structure of the zonal velocity at 450 m depth shows weaker and broader zonal jets when compared to TATL3, for example, (Figure A7). The biogeochemical model overestimates the size of the Atlantic OMZs, in particular the OMZ thickness in the coastal region. In addition, the impact of the westward zonal velocities in advecting the OMZ westward persists even in the 27-year average, as seen by the alternating bands of low oxygen. We note that the zonal velocities shown in Figure A7 are from the assimilative physical model. The biogeochemical model is coupled to a non-assimilative physical model, as previously mentioned. The lower oxygen concentrations in the OMZs than in the CARS climatology may be a consequence of the lack of oxygen supply from the western part of the basin by the zonal jets, inadequate representation of the eastern boundary current system, insufficient eddy variability at depth to redistribute tracers horizontally near the productive coastal regions and/or excessive biological production and respiration, as seen from the low values near the EBUS. In addition, larger oxygen concentrations on the western part of the basin as compared to the CARS climatology or TATL3 suggests that tracers are not redistributed properly at depth, which seems to be an inherent limitation of the low resolution of the model, as seen in TATL10.

In summary, the relatively low resolution precludes a realistic representation of alternating zonal jets and deeper mesoscale structures which affect tracer redistribution in the coastal and open ocean as well as the supply of oxygen to the OMZs. While data assimilation is extremely useful for a dynamically consistent monitoring of the state of the ocean and for medium-term forecast, intrinsic limitations due to low model resolution eventually arise, thus preventing a mechanistic understanding of the coupled physical-biogeochemical processes that modulate oxygen concentrations in the ocean.

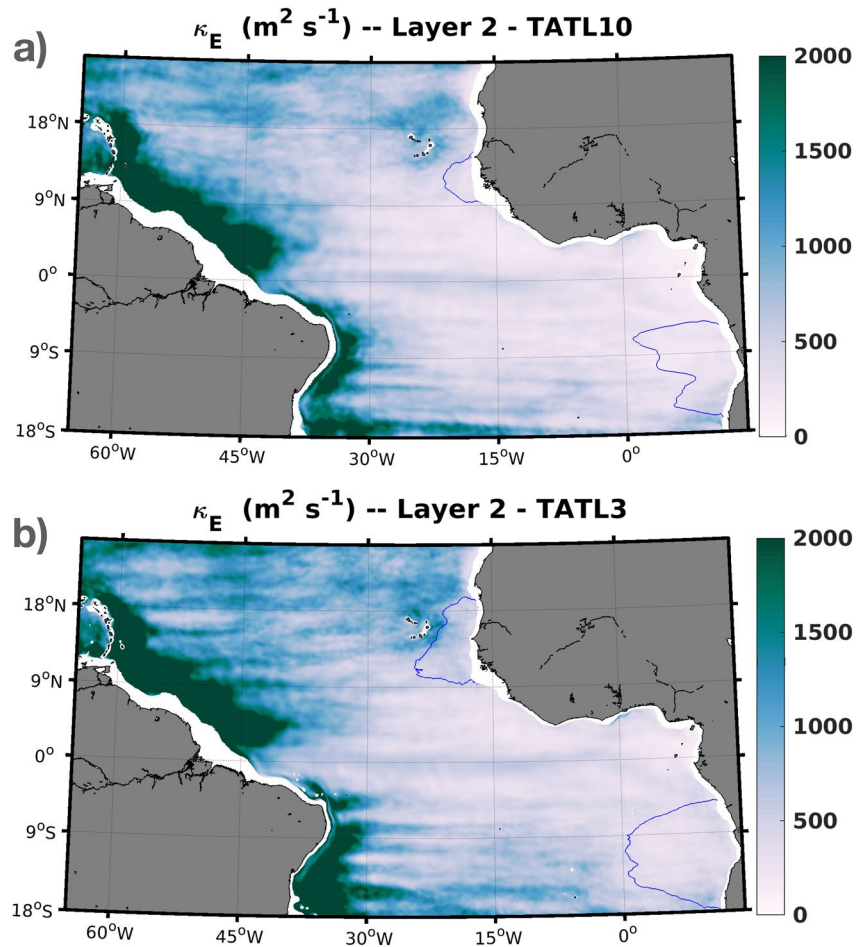


Figure 14. Eddy diffusivity calculated from averaged values in layer 2 for (a) TATL10 and (b) TATL3. The $80 \mu\text{mol L}^{-1}$ oxygen concentration isoline interpolated at this isopycnal surface is shown as a blue line.

6. Discussion and Conclusions

In this study, we used two physical-biogeochemical model configurations of the Tropical Atlantic, one at $1/10^\circ$ resolution, roughly the current highest horizontal resolution used in climate models and one at $1/30^\circ$ resolution. The increase in horizontal resolution produces more robust intermediate zonal jets which have a substantial impact on the Atlantic OMZs. The jets are more intensified on the western part of the basin, which is also where higher oxygen concentrations are observed. The eastward extent of the intermediate zonal jets delimits the western border of the OMZs. Within the OMZs, increased eddy variability at depth and a better representation of coastal and shelf current systems in the high-resolution run makes it more efficient in the horizontal redistribution of low-oxygen waters from the productive eastern boundaries.

Increased horizontal resolution and a relatively large domain allow the interplay of eddying and wave processes at multiple scales which lead to the emergence of robust, intermediate zonal jets (Kamenkovich et al., 2009; Lévy et al., 2010). In addition, numerical diffusivity is grid-size dependent, the higher the resolution the lower the numerical diffusivity. This may facilitate the formation of more robust zonal jets in high-resolution runs. Currently, the complexity of these motions and their impact on tracer transport is not fully captured in subgrid scale parameterizations (Kamenkovich et al., 2019, 2021). The anisotropy, spatial inhomogeneity and non-stationary of eddying motions, particularly at depth, seem to be relevant in this case.

The high resolution (3 km) run TATL3 produced a more robust field of alternating zonal jets down to 1,000 m. The stronger eastward jets impact the vertical structure of the OMZs by reducing the magnitude of the surface westward jets which in the low-resolution (10 km) run TATL10 carry low-oxygen waters from the OMZs and

distort their vertical structure by making them wider and thinner. Because the mostly wind-forced circulation in the upper 300 m is relatively similar in both runs, the westward jets have a strong impact on the OMZ as they are not counteracted by the deeper, eastward jets. The horizontal extent of the OMZs is determined by the longitude at which the eastward zonal jets weaken.

The oxygen budget below 200 m is dominated by advection, which is more important to the core of the ETNA OMZ than the ETSA OMZ. This could be due to the fact that the ETSA OMZ core is further away from the region of influence of the South Atlantic zonal jets because of the geometry of the basin. The implication for this would be that the core of the ETNA OMZ is more immediately sensitive to variations on the transport of the zonal jets. The ETSA OMZ is also known to be influenced by the variability of the Angola-Benguela Frontal Zone, which we do not fully simulate because of computational limitations in terms of domain size.

Vertical mixing is an important source of oxygen for the shallow OMZs at approximately 100 m depth. Deeper in the water column, the dominant balance is between biological consumption and advection although mixing is shown to have a small, positive contribution in the Atlantic OMZs. Eddy diffusivities are larger in TATL3 with larger values associated with the locations of the zonal jets. While the OMZs have lower eddy diffusivities, values also increase in TATL3 with similar contributions of both zonal and meridional eddy velocities.

While the comparison between TATL3 and TATL10 is mostly based on the different horizontal resolution, it is important to note that in sigma-coordinate (i.e., bathymetry-following) models such as CROCO, an increase in the horizontal resolution of the model grid also increases the bathymetry resolution which can impact vertical mixing rates particularly on the continental shelf/shelfbreak and regions with rough topography with consequences for tracer distribution.

The repeating, climatological wind and heat fluxes used to force the model runs in this study may cause the formation of the zonal jets at approximately the same latitudes so that they are more easily detected on the 7-year average. More realistic forcing with interannual variability (e.g., meridional shifts of the ITCZ) could generate meridional variations in the zonal jets so that such defined bands may not be so clear.

The biogeochemical coupling with the hydrodynamical model at different horizontal resolutions also raises questions about how resolution-dependent are biogeochemical parameters as well as about nonlinear feedbacks between oxygen consumption and production by the biology with different rates of supply and mixing by the physics.

This study shows that intermediate zonal jets have a significant impact on the supply of oxygen and the overall structure of the Atlantic OMZs and provides a pathway for an accurate representation of the OMZs and their intrinsic properties which are essential for the investigation of coastal and open ocean deoxygenation and its sensitivity to natural and anthropogenic forcing as well as for reliable long-term forecasts.

Appendix A: Model Evaluation

Normalized Taylor and target diagrams for salinity, temperature, oxygen and nitrate averaged at 250, 450 and 650 m depths are shown in Figures A2 and A3. These depths roughly correspond to the upper, core and lower parts of the OMZs, respectively. The regions used for the Taylor and target diagram calculation encompass large portions of the North and South Atlantic oceans, including the OMZs (the squares in Figure A1a). Overall, there is a general improvement in TATL3 for all variables, most notably for oxygen and nitrate. The skill of the simulations is better in the North Atlantic, which may be a consequence of a larger number of observations available in the climatology. In the South Atlantic, these variables may not be as well constrained as in its northern counterpart, particularly below 250 m depth. These metrics show that both simulations provide realistic representations of the averaged hydrographic conditions of both physical and biogeochemical variables. Figure A2, Figure A3, Figure A4, Figure A5, Figure A6, Figure A7.

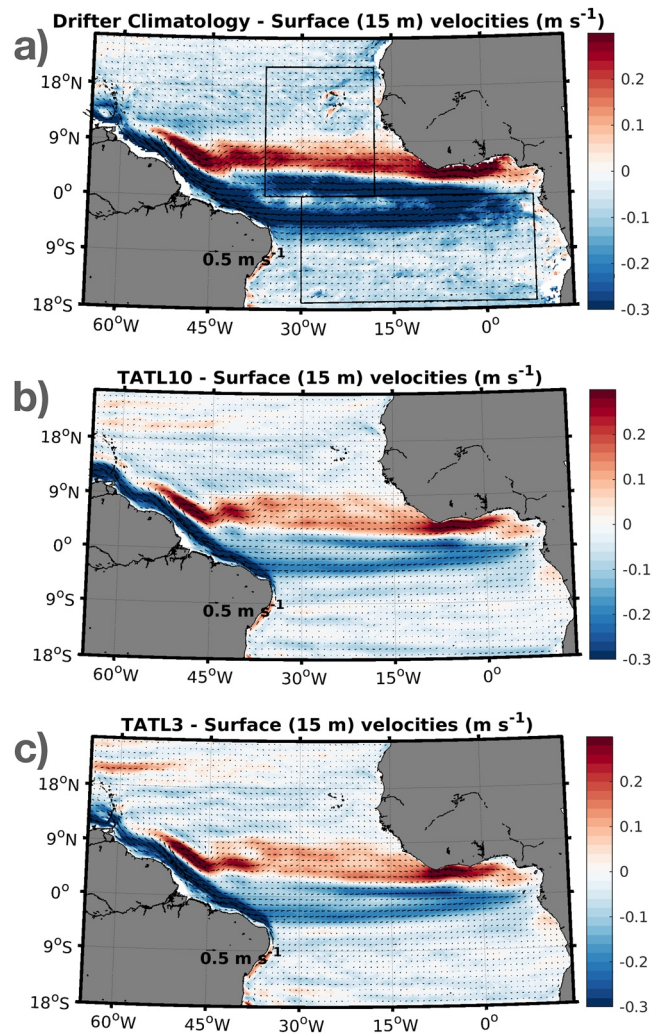


Figure A1. Comparison of surface velocities from TATL10 and TATL3 with a climatology from surface drifters obtained by Laurindo et al. (2017). Squares shown in (a) are the regions in the North and South Atlantic selected for computing Taylor and target diagrams shown in Figures A2 and A3.

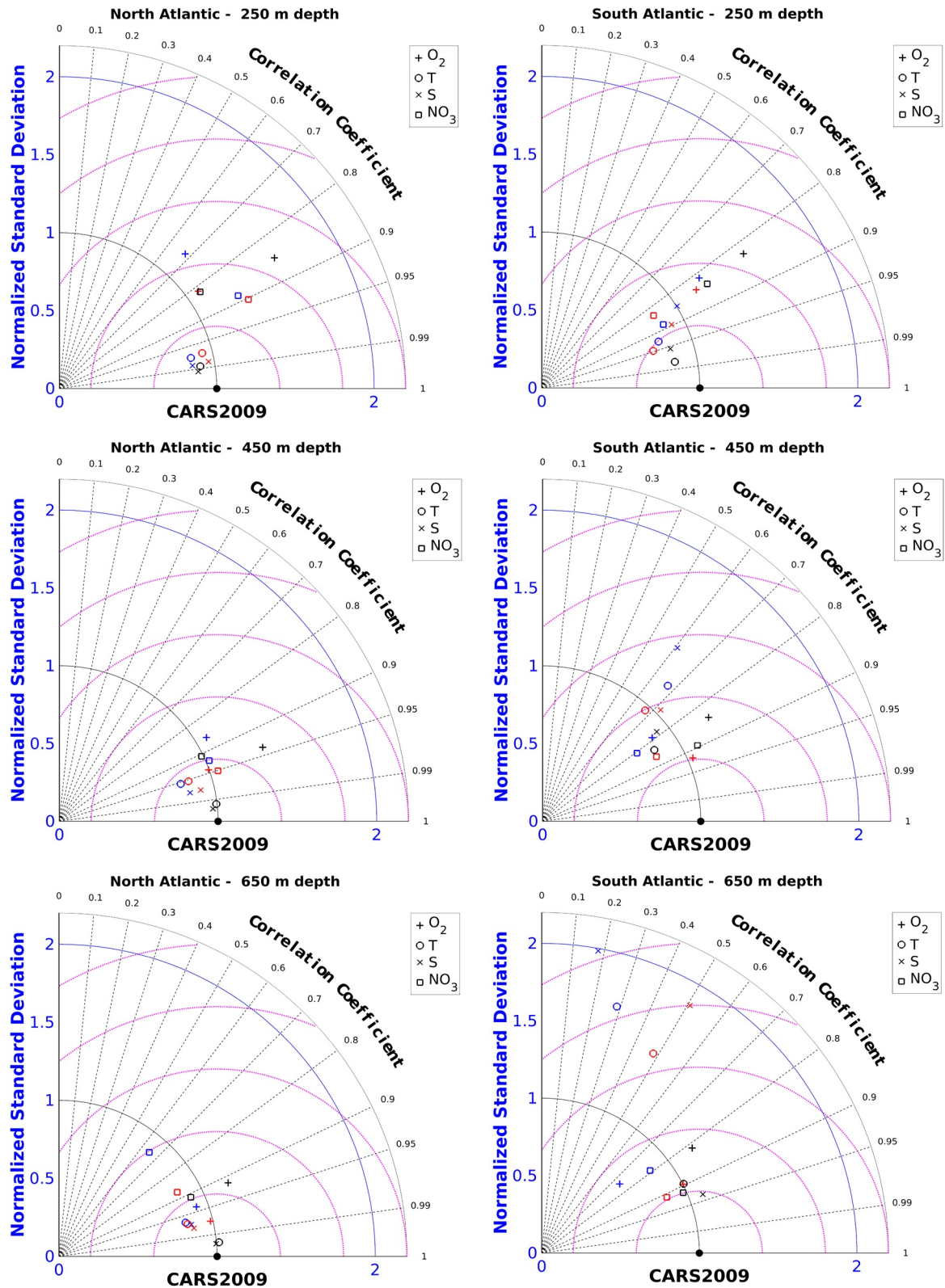


Figure A2. Normalized Taylor diagrams calculated at different depths in the North (left) and South (right) Atlantic subdomains for oxygen, nitrate, temperature and salinity in TATL10 (blue), TATL3 (red) and CMEMS (black). CMEMS models results are discussed in Section 5.

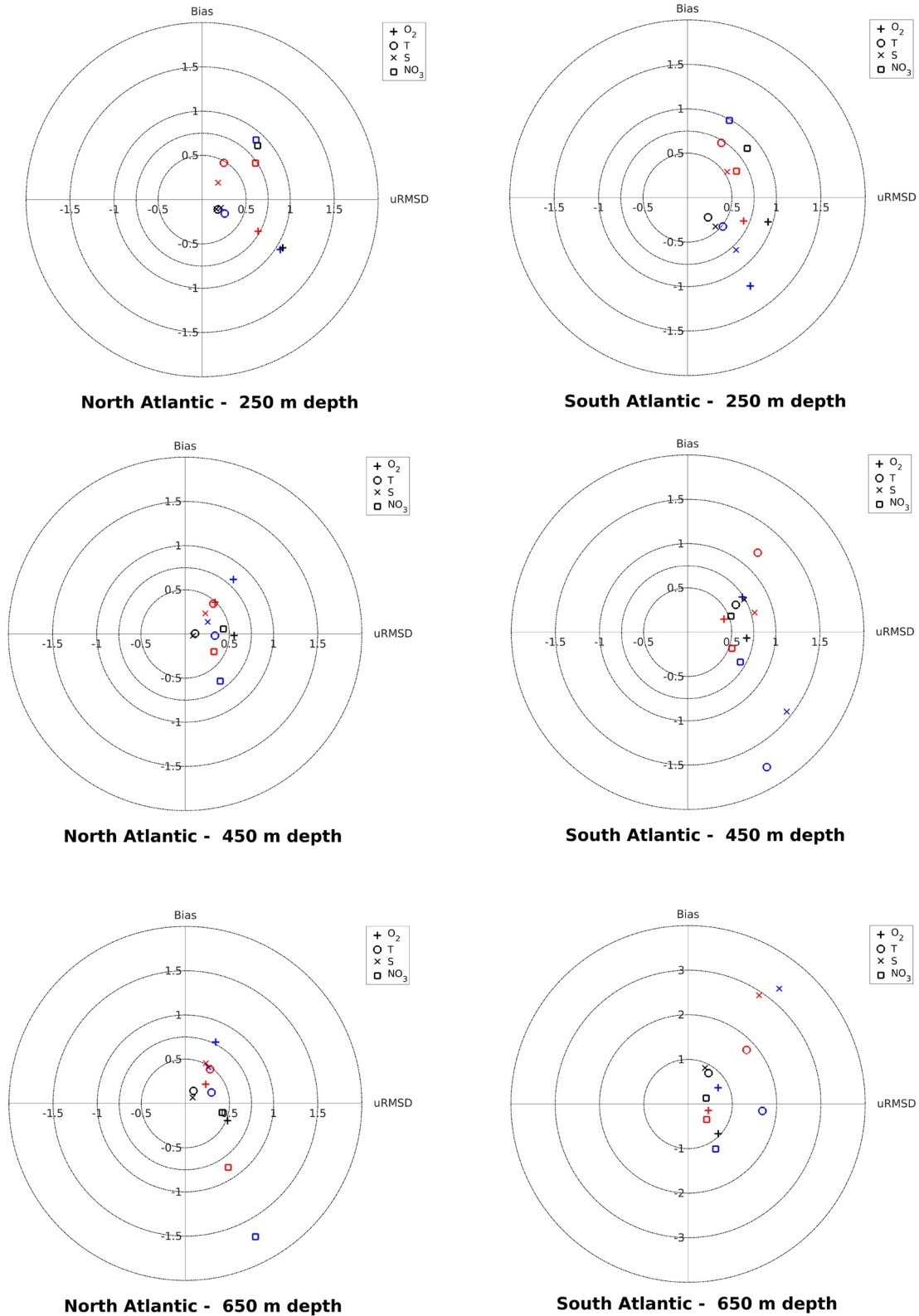


Figure A3. Target diagrams for averages of vertical sections for oxygen, nitrate, temperature and salinity in TATL10 (blue), TATL3 (red), and CMEMS (black). CMEMS models results are discussed in Section 5.

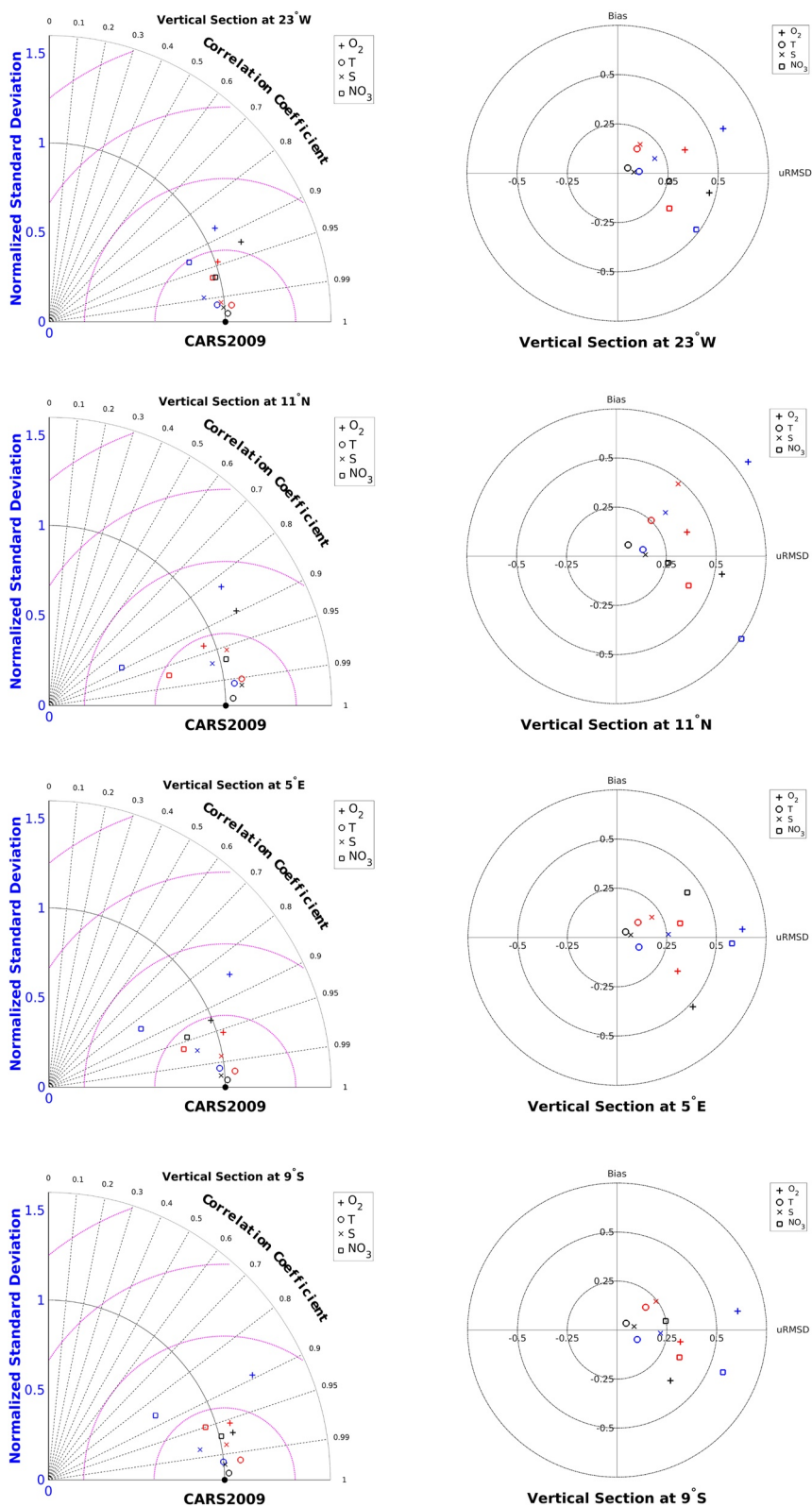


Figure A4. Target and Taylor diagrams for various vertical sections shown in the text. TATL10 (blue), TATL3 (red) and CMEMS (black). CMEMS models results are discussed in Section 5.

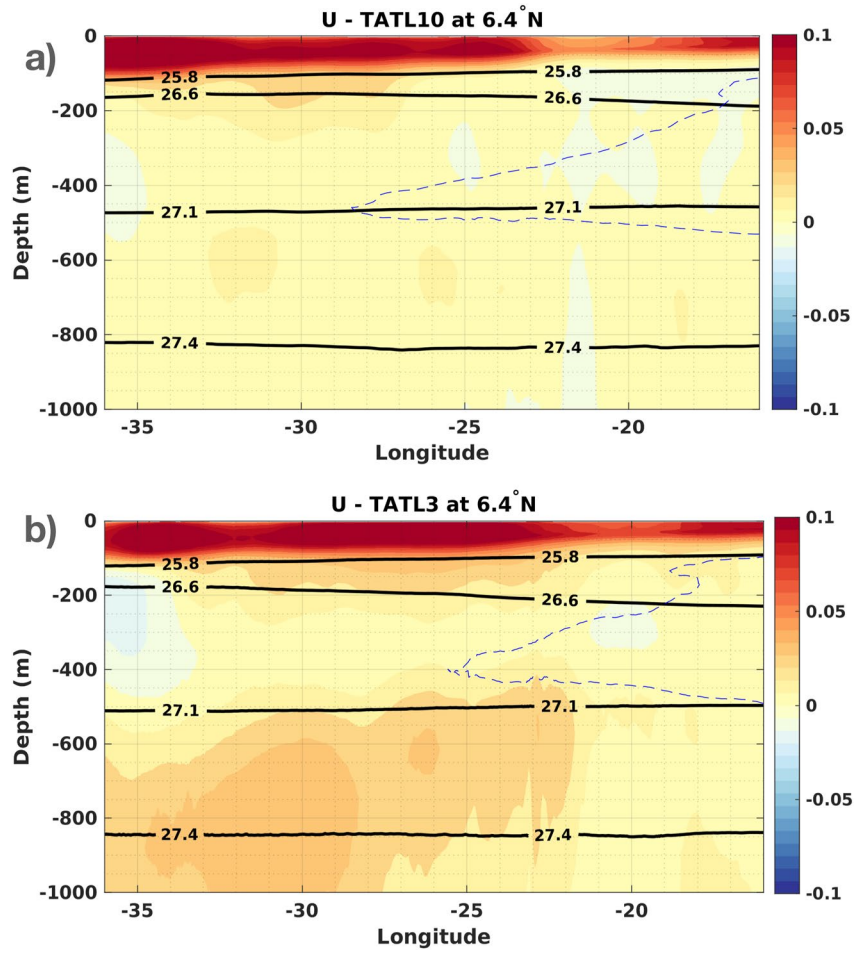


Figure A5. Zonal transect of 7-year averaged zonal velocities from (a) TATL10 and (b) TATL3 at 6.4°N. Isopycnal surfaces 25.8, 26.6, 27.1 and 27.4 kg m^{-3} are shown as black lines.

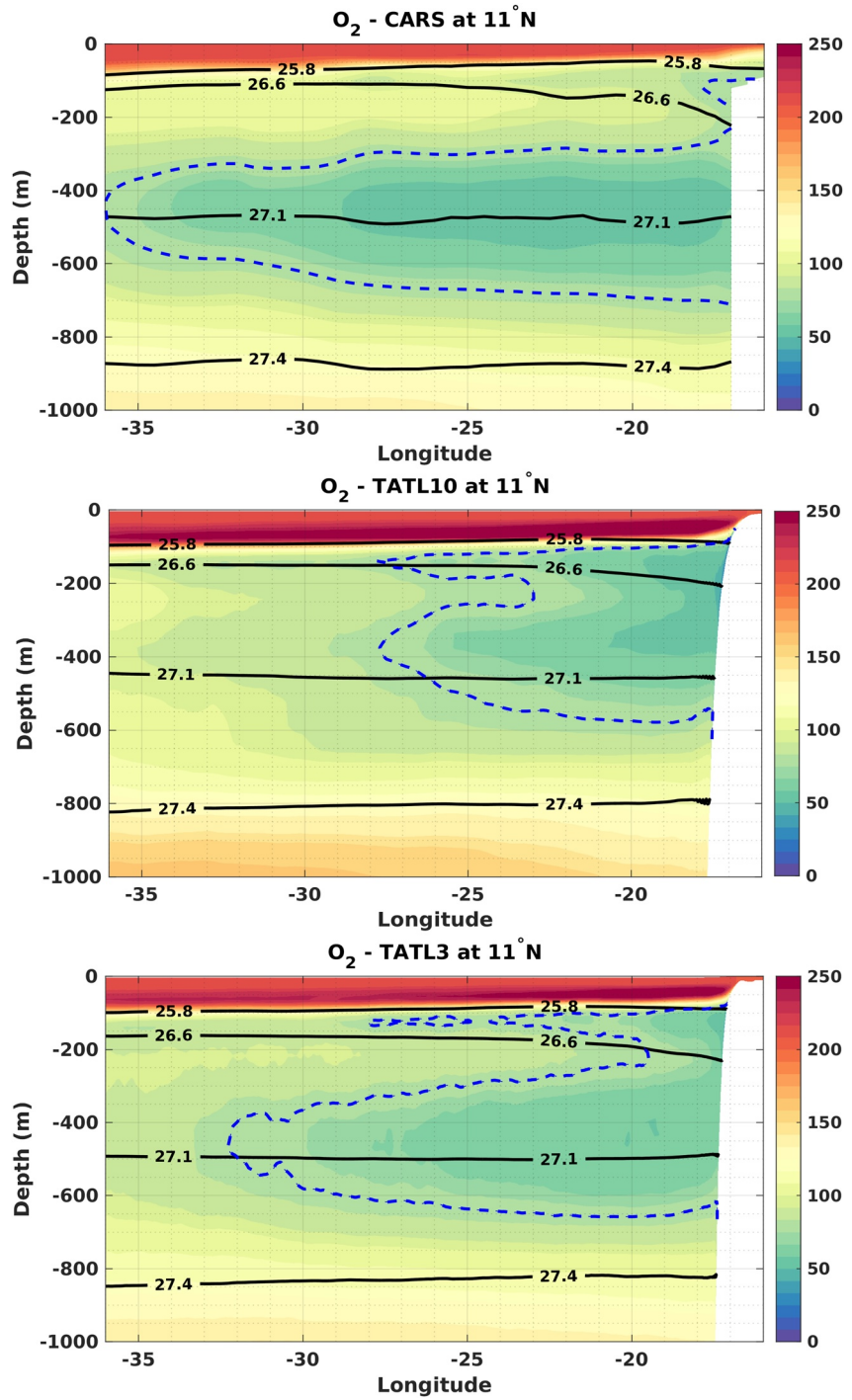


Figure A6. Zonal transect of climatological oxygen concentrations from (a) CARS and 7-year averages from (b) TATL10 and (c) TATL3 at 11°N. Isopycnal surfaces 25.8, 26.6, 27.1 and 27.4 kg m⁻³ are shown as black lines.

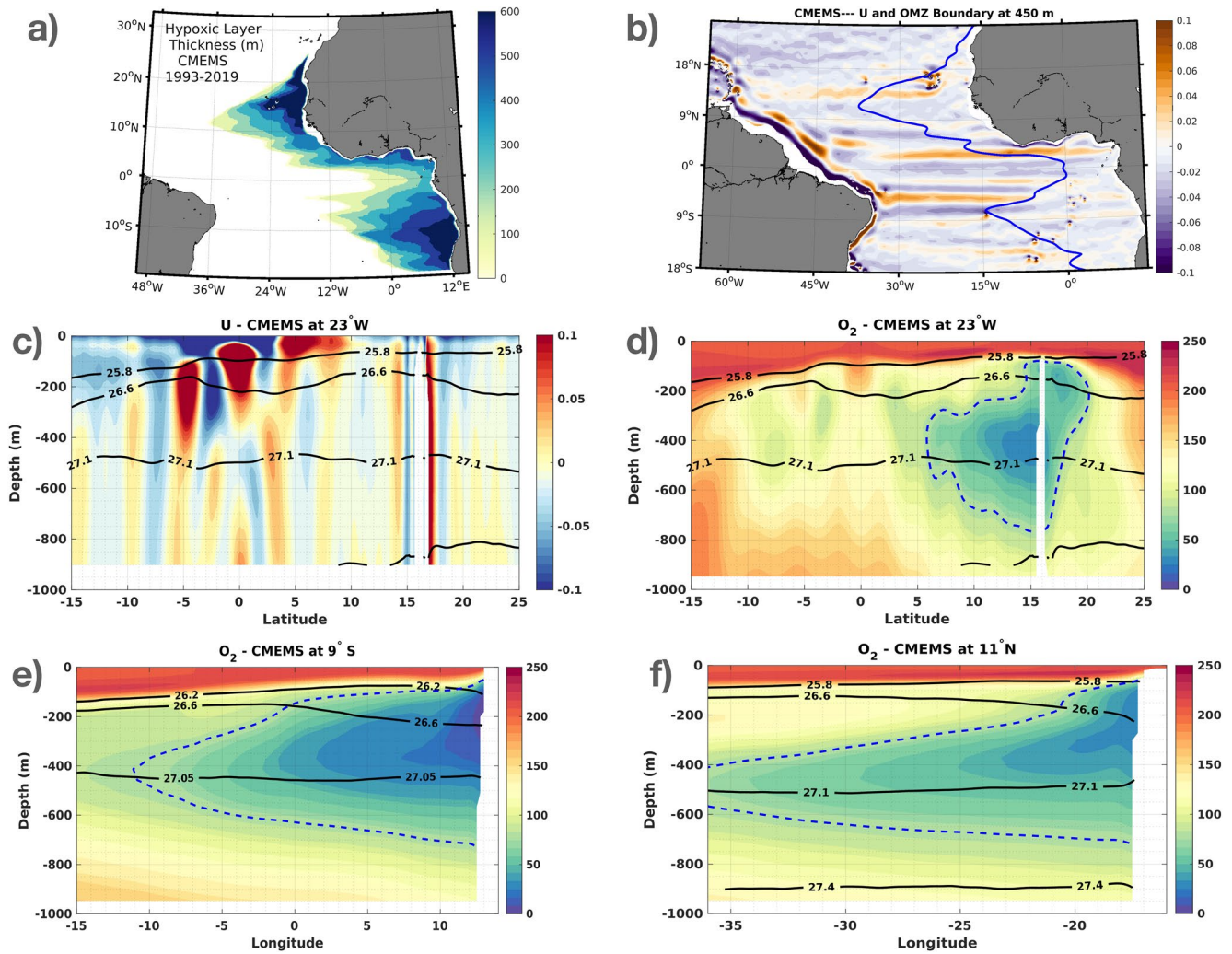


Figure A7. Averages from 1993 to 2019 obtained from two CMEMS model products: (a) hypoxic layer thickness, (b) zonal velocities at 450 m with the $80 \mu\text{mol L}^{-1}$ oxygen concentration isoline shown as a blue line, (c) zonal velocities at 23°W with isopycnal surfaces shown as black lines, (d) oxygen concentrations at 23°W with isopycnal surfaces shown as black lines, (e) averaged oxygen concentrations at 9°S and (f) 11°N .

Appendix B: Model Drift

Here we show the evolution of domain-averaged properties in the 7 years of model simulation (Figure B1). The domain-averaged model drift for each variable during the 7-years of model run is shown in Table B1.

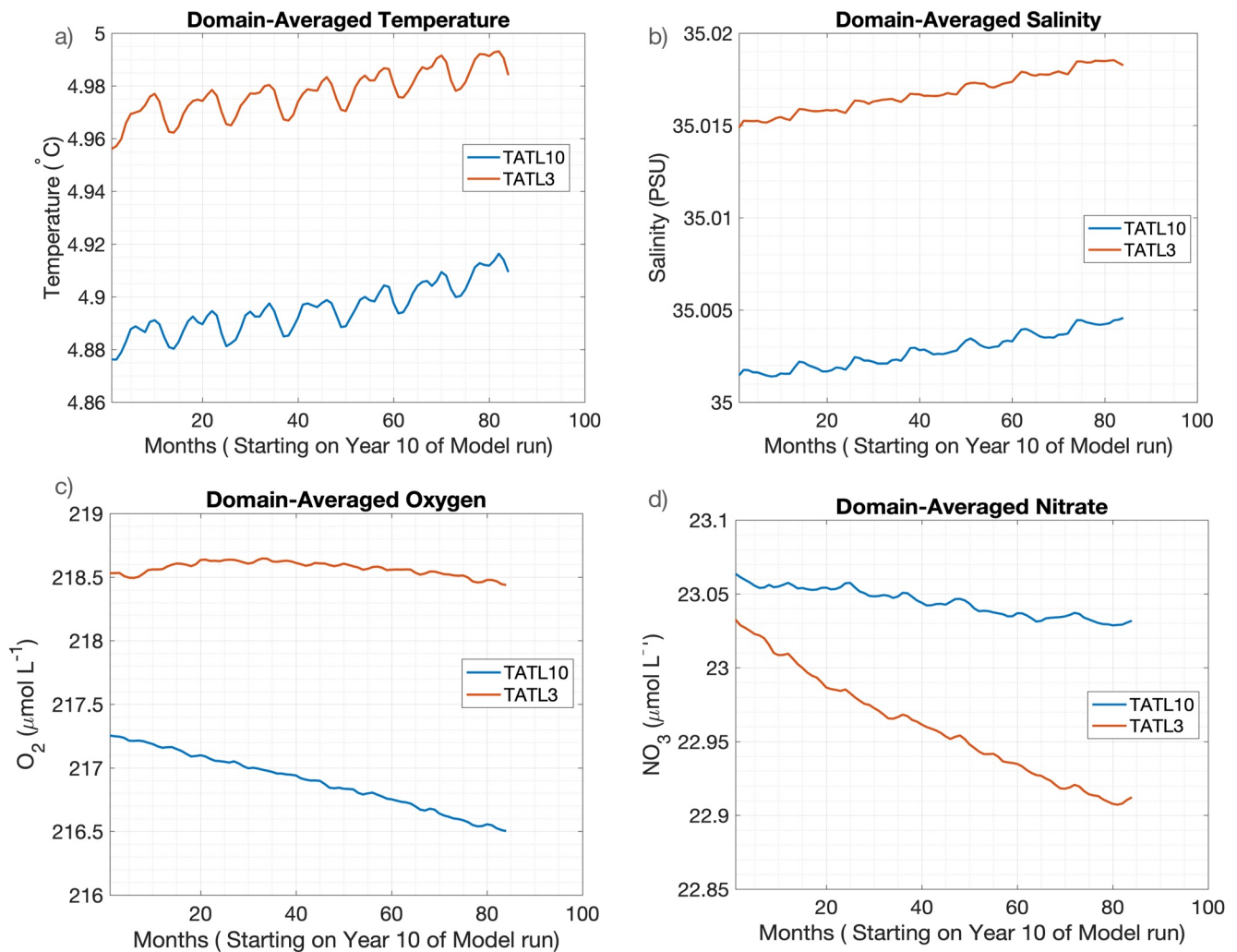


Figure B1. Domain-averaged model drift during the simulation period analyzed in this study.

Table B1 <i>Domain-Averaged Model Drift</i>		
Variable	TATL10	TATL3
Temperature (°C/year)	5.0×10^{-3}	4.0×10^{-3}
Salinity (PSU/year)	4.4×10^{-4}	4.8×10^{-4}
Oxygen ($\mu\text{mol L}^{-1}/\text{year}$)	-0.11	-0.01
Nitrate ($\mu\text{mol L}^{-1}$)	-5×10^{-3}	2×10^{-2}

Data Availability Statement

The data used in this study as well as the software required to reproduce the figures are available in (Calil, 2022a, 2022b). Scripts to used to plot the figures in this manuscript may be found in Calil (2022c).

Acknowledgments

The model simulations were performed on the HPC cluster Strand at Hereon. I thank the cluster team for the maintenance of system. I would like to thank Laure Resplandy for detailed review comments which significantly improved the manuscript. I would also like to thank Eric Firing, Ryo Furue and Dante Napolitano for comments provided on an earlier version of the manuscript. ROMS model variables were interpolated into isopycnal surfaces using a C++ program written by Lucas Merckelbach (Hereon) and available at <https://github.com/smerckel/isopycnal-interpolation>. Open Access funding enabled and organized by Projekt DEAL.

References

- Assene, F., Morel, Y., Delpech, A., Aguedjou, M., Jouanno, J., Cravatte, S., et al. (2020). From mixing to the large scale circulation: How the inverse cascade is involved in the formation of the subsurface currents in the Gulf of Guinea. *Fluids*, 5(3), 147. <https://doi.org/10.3390/fluids5030147>
- Aumont, O., & Bopp, L. (2006). Globalizing results from ocean in situ iron fertilization studies. *Global Biogeochemical Cycles*, 20(2). <https://doi.org/10.1029/2005gb002591>
- Aumont, O., Maier-Reimer, E., Blain, S., & Monfray, P. (2003). An ecosystem model of the global ocean including fe, si, p colimitations. *Global Biogeochemical Cycles*, 17(2). <https://doi.org/10.1029/2001gb001745>
- Banyte, D., Visbeck, M., Tanhua, T., Fischer, T., Krahnmann, G., & Karstensen, J. (2013). Lateral diffusivity from tracer release experiments in the Tropical North Atlantic thermocline. *Journal of Geophysical Research: Oceans*, 118(5), 2719–2733. <https://doi.org/10.1002/jgrc.20211>
- Brandt, P., Bange, H. W., Banyte, D., Dengler, M., Didwischus, S.-H., Fischer, T., et al. (2015). On the role of circulation and mixing in the ventilation of oxygen minimum zones with a focus on the eastern Tropical North Atlantic. *Biogeosciences*, 12(2), 489–512. <https://doi.org/10.5194/bg-12-489-2015>
- Brandt, P., Greatbatch, R. J., Claus, M., Didwischus, S.-H., Hormann, V., Funk, A., et al. (2012). Ventilation of the equatorial Atlantic by the equatorial deep jets. *Journal of Geophysical Research*, 117(C12), C12015. <https://doi.org/10.1029/2012jc008118>
- Brandt, P., Hahn, J., Schmidt, S., Tuchen, F. P., Kopte, R., Kiko, R., et al. (2021). Atlantic equatorial undercurrent intensification counteracts warming-induced deoxygenation. *Nature Geoscience*, 14(5), 278–282. <https://doi.org/10.1038/s41561-021-00716-1>
- Brandt, P., Hormann, V., Bourles, B., Fischer, J., Schott, F. A., Stramma, L., & Dengler, M. (2008). Oxygen tongues and zonal currents in the equatorial Atlantic. *Journal of Geophysical Research*, 113(C4), C04012. <https://doi.org/10.1029/2007jc004435>
- Brandt, P., Hormann, V., Körtzinger, A., Visbeck, M., Krahnmann, G., Stramma, L., et al. (2010). Changes in the ventilation of the oxygen minimum zone of the tropical north Atlantic. *Journal of Physical Oceanography*, 40(8), 1784–1801. <https://doi.org/10.1175/2010jpo4301.1>
- Breitburg, D., Levin, L. A., Oschlies, A., Grégoire, M., Chavez, F. P., Conley, D. J., et al. (2018). Declining oxygen in the global ocean and coastal waters. *Science*, 359(6371). <https://doi.org/10.1126/science.aam7240>
- Bryden, H. L., McDonagh, E. L., & King, B. A. (2003). Changes in ocean water mass properties: Oscillations or trends? *Science*, 300(5628), 2086–2088. <https://doi.org/10.1126/science.1083980>
- Burmeister, K., Lübbecke, J. F., Brandt, P., & Duteil, O. (2019). Interannual variability of the Atlantic north equatorial undercurrent and its impact on oxygen. *Journal of Geophysical Research: Oceans*, 124(4), 2348–2373. <https://doi.org/10.1029/2018jc014760>
- Busecke, J. J., Resplandy, L., & Dunne, J. P. (2019). The equatorial undercurrent and the oxygen minimum zone in the Pacific. *Geophysical Research Letters*, 46(12), 6716–6725. <https://doi.org/10.1029/2019gl082692>
- Cabr e, A., Marinov, I., Bernardello, R., & Bianchi, D. (2015). Oxygen minimum zones in the tropical Pacific across CMIP5 models: Mean state differences and climate change trends. *Biogeosciences*, 12(18), 5429–5454. <https://doi.org/10.5194/bg-12-5429-2015>
- Calil, P. (2022a). Datasets for “high-resolution, basin-scale simulations reveal the impact of intermediate zonal jets on the Atlantic oxygen minimum zones”- Part 1 [dataset]. Zenodo. <https://doi.org/10.5281/zenodo.7229219>
- Calil, P. (2022b). Datasets for “high-resolution, basin-scale simulations reveal the impact of intermediate zonal jets on the Atlantic oxygen minimum zones”- Part 2 [dataset]. Zenodo. <https://doi.org/10.5281/zenodo.7081664>
- Calil, P. (2022c). m-files required for the reproduction of figures shown in “high-resolution, basin-scale simulations reveal the impact of intermediate zonal jets on the atlantic oxygen minimum zones” [software]. Zenodo. <https://doi.org/10.5281/zenodo.7234366>
- Carton, J. A., Chepurin, G. A., & Chen, L. (2018). SODA3: A new ocean climate reanalysis. *Journal of Climate*, 31(17), 6967–6983. <https://doi.org/10.1175/jcli-d-18-0149.1>
- Chassignet, E. P., & Xu, X. (2017). Impact of horizontal resolution (1/12 to 1/50s) on Gulf Stream Separation, penetration, and variability. *Journal of Physical Oceanography*, 47(8), 1999–2021. <https://doi.org/10.1175/jpo-d-17-0031.1>
- Cornillon, P. C., Firing, E., Thompson, A. F., Ivanov, L. M., Kamenkovich, I., Buckingham, C. E., & Afanasyev, Y. D. (2019). Oceans. In B. Galperin & P. L. Read (Eds.), *Zonal jets: Phenomenology, genesis, and physics* (pp. 46–71). Cambridge University Press. <https://doi.org/10.1017/9781107358225.003>
- Czeschel, R., Stramma, L., Schwarzkopf, F. U., Giese, B. S., Funk, A., & Karstensen, J. (2011). Middepth circulation of the eastern tropical south Pacific and its link to the oxygen minimum zone. *Journal of Geophysical Research*, 116(C1), C01015. <https://doi.org/10.1029/2010jc006565>
- Czeschel, R., Stramma, L., Weller, R., & Fischer, T. (2015). Circulation, eddies, oxygen, and nutrient changes in the eastern tropical south Pacific Ocean. *Ocean Science*, 11(3), 455–470. <https://doi.org/10.5194/os-11-455-2015>
- Delpech, A., Cravatte, S., Marin, F., Morel, Y., Gronchi, E., & Kestenare, E. (2020). Observed tracer fields structuration by middepth zonal jets in the tropical Pacific. *Journal of Physical Oceanography*, 50(2), 281–304. <https://doi.org/10.1175/jpo-d-19-0132.1>
- Doney, S. C., Lima, I., Moore, J. K., Lindsay, K., Behrenfeld, M. J., Westberry, T. K., et al. (2009). Skill metrics for confronting global upper ocean ecosystem-biogeochemistry models against field and remote sensing data. *Journal of Marine Systems*, 76(1–2), 95–112. <https://doi.org/10.1016/j.jmarsys.2008.05.015>
- Duteil, O., Schwarzkopf, F. U., Böning, C. W., & Oschlies, A. (2014). Major role of the equatorial current system in setting oxygen levels in the eastern tropical Atlantic Ocean: A high-resolution model study. *Geophysical Research Letters*, 41(6), 2033–2040. <https://doi.org/10.1002/2013gl058888>
- Eden, C. (2006). Middepth equatorial tracer tongues in a model of the Atlantic Ocean. *Journal of Geophysical Research*, 111(C12), C12025. <https://doi.org/10.1029/2006jc003565>
- Eden, C., & Greatbatch, R. J. (2008). Diapycnal mixing by meso-scale eddies. *Ocean Modelling*, 23(3–4), 113–120. <https://doi.org/10.1016/j.ocemod.2008.04.006>
- Frenger, I., Bianchi, D., Stührenberg, C., Oschlies, A., Dunne, J., Deutsch, C., et al. (2018). Biogeochemical role of subsurface coherent eddies in the ocean: Tracer cannonballs, hypoxic storms, and microbial stewpots? *Global Biogeochemical Cycles*, 32(2), 226–249. <https://doi.org/10.1002/2017gb005743>
- Gordon, A. L., & Bosley, K. T. (1991). Cyclonic gyre in the tropical South Atlantic. *Deep-Sea Research, Part A: Oceanographic Research Papers*, 38, S323–S343. [https://doi.org/10.1016/s0198-0149\(12\)80015-x](https://doi.org/10.1016/s0198-0149(12)80015-x)
- Hahn, J., Brandt, P., Greatbatch, R. J., Krahnmann, G., & Körtzinger, A. (2014). Oxygen variance and meridional oxygen supply in the tropical north east Atlantic oxygen minimum zone. *Climate Dynamics*, 43(11), 2999–3024. <https://doi.org/10.1007/s00382-014-2065-0>
- Huang, H.-P., Kaplan, A., Curchitser, E. N., & Maximenko, N. A. (2007). The degree of anisotropy for mid-ocean currents from satellite observations and an eddy-permitting model simulation. *Journal of Geophysical Research*, 112(C9), C09005. <https://doi.org/10.1029/2007jc004105>
- Jolliff, J. K., Kindle, J. C., Shulman, I., Penta, B., Friedrichs, M. A., Helber, R., & Arnone, R. A. (2009). Summary diagrams for coupled hydrodynamic-ecosystem model skill assessment. *Journal of Marine Systems*, 76(1–2), 64–82. <https://doi.org/10.1016/j.jmarsys.2008.05.014>

- Kamenkovich, I., Berloff, P., Haigh, M., Sun, L., & Lu, Y. (2021). Complexity of mesoscale eddy diffusivity in the ocean. *Geophysical Research Letters*, 48(5), e2020GL091719. <https://doi.org/10.1029/2020gl091719>
- Kamenkovich, I., Berloff, P., & Pedlosky, J. (2009). Role of eddy forcing in the dynamics of multiple zonal jets in a model of the north Atlantic. *Journal of Physical Oceanography*, 39(6), 1361–1379. <https://doi.org/10.1175/2008jpo4096.1>
- Kamenkovich, I., Berloff, P., & Rypina, I. I. (2019). Anisotropic and inhomogeneous eddy-induced transport in flows with jets. In B. Galperin & P. L. Read (Eds.), *Zonal jets: Phenomenology, genesis, and physics* (pp. 437–449). Cambridge University Press. <https://doi.org/10.1017/9781107358225.028>
- Karstensen, J., Stramma, L., & Visbeck, M. (2008). Oxygen minimum zones in the eastern tropical Atlantic and Pacific oceans. *Progress in Oceanography*, 77(4), 331–350. <https://doi.org/10.1016/j.pocean.2007.05.009>
- Kopte, R., Brandt, P., Dengler, M., Tchikalanga, P., Macuéria, M., & Ostrowski, M. (2017). The Angola current: Flow and hydrographic characteristics as observed at 11 s. *Journal of Geophysical Research: Oceans*, 122(2), 1177–1189. <https://doi.org/10.1002/2016jc012374>
- Kwiatkowski, L., Torres, O., Bopp, L., Aumont, O., Chamberlain, M., Christian, J. R., et al. (2020). Twenty-first century ocean warming, acidification, deoxygenation, and upper-ocean nutrient and primary production decline from CMIP6 model projections. *Biogeosciences*, 17(13), 3439–3470. <https://doi.org/10.5194/bg-17-3439-2020>
- Laurindo, L. C., Mariano, A. J., & Lumpkin, R. (2017). An improved near-surface velocity climatology for the global ocean from drifter observations. *Deep Sea Research Part I: Oceanographic Research Papers*, 124, 73–92. <https://doi.org/10.1016/j.dsr.2017.04.009>
- Levin, L. A. (2018). Manifestation, drivers, and emergence of open ocean deoxygenation. *Annual Review of Marine Science*, 10(1), 229–260. <https://doi.org/10.1146/annurev-marine-121916-063359>
- Lévy, M., Klein, P., Tréguier, A.-M., Iovino, D., Madec, G., Masson, S., & Takahashi, K. (2010). Modifications of gyre circulation by sub-mesoscale physics. *Ocean Modelling*, 34(1–2), 1–15. <https://doi.org/10.1016/j.ocemod.2010.04.001>
- Lévy, M., Resplandy, L., Palter, J. B., Couespel, D., & Lachkar, Z. (2022). The crucial contribution of mixing to present and future ocean oxygen distribution. In *Ocean mixing* (pp. 329–344). Elsevier.
- Marchesiello, P., Debreu, L., & Couvelard, X. (2009). Spurious diapycnal mixing in terrain-following coordinate models: The problem and a solution. *Ocean Modelling*, 26(3–4), 156–169. <https://doi.org/10.1016/j.ocemod.2008.09.004>
- Maximenko, N. A., Bang, B., & Sasaki, H. (2005). Observational evidence of alternating zonal jets in the world ocean. *Geophysical Research Letters*, 32(12), L12607. <https://doi.org/10.1029/2005gl022728>
- Maximenko, N. A., Melnichenko, O. V., Niiler, P. P., & Sasaki, H. (2008). Stationary mesoscale jet-like features in the ocean. *Geophysical Research Letters*, 35(8), L08603. <https://doi.org/10.1029/2008gl033267>
- Monteiro, P., Van Der Plas, A., Melice, J.-L., & Florenchie, P. (2008). Interannual hypoxia variability in a coastal upwelling system: Ocean–shelf exchange, climate and ecosystem-state implications. *Deep Sea Research Part I: Oceanographic Research Papers*, 55(4), 435–450. <https://doi.org/10.1016/j.dsr.2007.12.010>
- Nakano, H., & Hasumi, H. (2005). A series of zonal jets embedded in the broad zonal flows in the Pacific obtained in eddy-permitting ocean general circulation models. *Journal of Physical Oceanography*, 35(4), 474–488. <https://doi.org/10.1175/jpo2698.1>
- Oschlies, A., Brandt, P., Stramma, L., & Schmidtko, S. (2018). Drivers and mechanisms of ocean deoxygenation. *Nature Geoscience*, 11(7), 467–473. <https://doi.org/10.1038/s41561-018-0152-2>
- Resplandy, L., Lévy, M., Madec, G., Pous, S., Aumont, O., & Kumar, D. (2011). Contribution of mesoscale processes to nutrient budgets in the Arabian Sea. *Journal of Geophysical Research*, 116(C11), C11007. <https://doi.org/10.1029/2011jc007006>
- Richards, K., Maximenko, N., Bryan, F., & Sasaki, H. (2006). Zonal jets in the Pacific Ocean. *Geophysical Research Letters*, 33(3), L03605. <https://doi.org/10.1029/2005gl024645>
- Stramma, L., Johnson, G. C., Sprintall, J., & Mohrholz, V. (2008). Expanding oxygen-minimum zones in the tropical oceans. *Science*, 320(5876), 655–658. <https://doi.org/10.1126/science.1153847>
- Tchikalanga, P., Dengler, M., Brandt, P., Kopte, R., Macuéria, M., Coelho, P., et al. (2018). Eastern boundary circulation and hydrography off Angola: Building Angolan oceanographic capacities. *Bulletin of the American Meteorological Society*, 99(8), 1589–1605. <https://doi.org/10.1175/bams-d-17-0197.1>
- Thomsen, S., Karstensen, J., Kiko, R., Krahnemann, G., Dengler, M., & Engel, A. (2019). Remote and local drivers of oxygen and nitrate variability in the shallow oxygen minimum zone off Mauritania in June 2014. *Biogeosciences*, 16(5), 979–998. <https://doi.org/10.5194/bg-16-979-2019>